J Comput Aided Mol Des (2011) 25:81–101
DOI 10.1007/s10822-010-9404-y

Molecular and structural determinants of adamantyl susceptibility to HLA-DRs allelic variants: an in silico approach to understand the mechanism of MLEs

Zaheer-ul-Haq · Waqasuddin Khan

Received: 28 August 2010 / Accepted: 14 November 2010 / Published online: 30 November 2010

Abstract Class II major histocompatibility complex (MHC II) molecules as expressed by antigen-presenting cells are heterodimeric cell-surface glycoprotein receptors that are fundamental in initiating and propagating an immune response by presenting tumor-associated antigenic peptides to $CD4^{+}/T_{H}$ cells. The loading efficiency of such peptides can be improved by small organic compounds (MHC Loading Enhancers—MLEs), that convert the non-receptive peptide conformation of MHC II to a peptide-receptive conformation. In a reversible reaction, these compounds open up the binding site of MHC II molecules by specific interactions with a yet undefined pocket. Here, we performed molecular docking and molecular dynamics simulation studies of adamantyl compounds on the predicted cavity around the P1 pocket of 2 allelic variants of HLA-DRs. The purpose was to investigate the suitability of adamantyl compounds as MLEs at the dimorphic β86 position. Docking studies revealed that besides numerous molecular interactions formed by the adamantyl compounds, Asnβ82, Tyrβ83, and Thrβ90 are the crucial amino acid residues that are characterized as the "sensors" of peptide loading. Molecular dynamics simulation studies exposed the dynamical structural changes that HLA-DRs adopted as a response to binding of 3-(1-adamantyl)-5-hydrazidocarbonyl-1H-pyrazole (AdCaPy). The conformations of AdCaPy complexed with the Glyβ86 HLA-DR allelic variant are well correlated with the stabilized form of peptide-loaded HLA-DRs, further confirming the role of AdCaPy as a MLE. Hydrogen bonding interaction analysis clearly demonstrated that after making suitable contacts with AdCaPy, HLA-DR changes its local conformation. However, AdCaPy complexed with HLA-DR having Valβ86 at the dimorphic position did not accommodate AdCaPy as MLE due to steric hindrance caused by the valine.

Keywords Major histocompatibility complex · Human leucocytes antigen · Polymorphism · Adamantyl compounds · Docking · Molecular dynamics simulation

Zaheer-ul-Haq (✉)
Dr. Panjwani Center for Molecular Medicine and Drug Research, International Center for Chemical and Biological Sciences, University of Karachi, Karachi 75270, Pakistan
e-mail: zaheer.qasmi@iccs.edu

W. Khan
H.E.J. Research Institute of Chemistry, International Center for Chemical and Biological Sciences, University of Karachi, Karachi 75270, Pakistan

Introduction

Class II major histocompatibility complex (MHC) molecules are heterodimeric cell-surface glycoprotein receptors that recognize and bind tumor-associated antigenic (TAA) peptides, as part of the adaptive immune response, having immunogenic determinants for the discrimination by T cells ($CD4^{+}/T_{H}$) [1]. Since after recognition by $CD4^{+}$ cells, specific MHC-TAA peptide complexes can trigger the destruction of a tumor cell, thus they have become a focal point for experimental tumor immune therapies. The loading efficiency of peptide tumor antigens can be improved by small organic compounds, MHC Loading Enhancers (MLEs), which operate by converting the peptide non-receptive conformation of MHC molecules into the peptide-receptive conformation. MLEs also act as mediators of T cell responses by promoting efficient transfer of a particular TAA peptide onto MHC molecules, so they are also involved in ligand-exchange catalysis.

Furthermore, these molecules bind peptides derived from endosomes or the extracellular milieu via the default endosomal pathway [2, 3]. Available crystal structures of different allelic variants bound to a variety of peptides have revealed a conserved hydrogen bonding network formed between the conserved amino acid residues in MHC II proteins (the anchored amino acid residues) and the peptide main chain carbonyl and amide groups. These interactions are accessible along the helices of alpha and beta peptide binding domain [4]. Furthermore, binding is mediated by the interaction of peptide side chains and MHC II pockets within the binding groove of the peptide-binding domain. Within this binding region, high side chain preferences are found at certain pockets or shelves with weaker preferences to others. Many of the residues that line these pockets are highly polymorphic, and thus lead to remarkable diversity within the peptide repertoire. Generally, these pockets accommodate side chains from the peptide residue at P1, P4, P6 and P9 positions, with smaller pockets or shelves in the binding site accommodating the P3 and P7 residues. These pockets are numbered along the N-terminal peptide relative to a large, usually hydrophobic pocket near the peptide binding site. For HLA-DR1 (DRB1*0101), a common human class II MHC protein and the subject of this study, has a P1 pocket that exhibits a strong preference for large hydrophobic side chains (Trp, Tyr, Phe, Leu and Ile), the P6 pocket has a strong preference for smaller residues (Gly, Ala, Ser and Pro) and the P4 and P9 pockets have weaker preference for residues with some aliphatic character [5]. Specifically, the P1 pocket appears to be modulated by Gly/Val dimorphism [6] that alters the preference towards smaller side chains. The substitution of Glyβ86 by valine would place the side chain of valine within the region occupied by a peptide side chain residue, and would restrict the size of the peptide side chain that can be accommodated at this position. Therefore, this position determines the allele-specific preferences for anchor residues.

Studies have shown that structural variations or alternate conformations are observed among numerous MHC II peptide-free and MHC II-peptide complexes. Several conformational-sensitive monoclonal antibodies (mAbs) such as mAb 64-3-7 [7], MEM-264 [8, 9], and bacterial superantigen—Staphylococcal Enterotoxin C3 (SEC3) [9] specifically detect open MHC II conformers by recognizing analogous MHC segments residues, β53–67 and another in the lower Ig-like domain (residues β186–189), as the molecular chaperone HLA-DM detected (a naturally occurring catalyst for peptide-exchange of MHC II). An antibody (KL295) restricted for the β58–69 region preferentially bound the empty MHC II protein, but not to the peptide-loaded MHC II protein, demonstrating that the peptide-induced conformational change involves the β-subunit helical region [10]. Peptide binding to MHC II causes a large decrease (10–15%) in the hydrodynamic radius of the protein as determined by gel filtration, dynamic light scattering, and analytical ultracentrifugation experiments. Adjustments in the MHC II polypeptide backbone structure as determined by circular dichroism are also observed indicating a decrease in helicity. This change is reversed upon peptide binding reflecting a trapping mechanism for bound peptide [10]. These studies helped to identify regions within the structure that change after peptide loading. Such changes can be induced by binding a wide variety of peptides regardless of peptide length, affinity, or sequence characteristics, provided that the P1 site is occupied [11].

Peptide binding and dissociation experiments have shown that MHC II protein can assume two inter-converting forms, one is the peptide-receptive state while other is the peptide non-receptive state [12]. The peptide-receptive state is competent to bind peptide rapidly. But in other case, if it is not stabilized by peptide or associated with the chaperone HLA-DM, it convert itself to peptide non-receptive form immediately. However, in contrast to this situation, conversion between non-receptive to receptive state of MHC II molecules is slow ($\sim 10^{-3}$ to 10^{-5} s^{-1}) and could involve formation of nonproductive species such as complexes carrying peptides bound in an inappropriate register or conformation [13]. In principle, the conversion between the two forms is reversible, but the equilibrium is largely shifted towards the non-receptive conformation.

The exquisite specificity of antigen recognition by the T cell arm of the immune response provides an important basis for cancer immunotherapy. Indeed, the isolation of tumor-specific $CD4^+$ cells from cancer patients has fueled the search for tumor-associated antigens. The induction of optimal systemic antitumor immunity involves the priming of both $CD4^+$ and $CD8^+$ T cells specific for tumor-associated antigens. The role of $CD4^+$ cells in this response has been largely attributed to providing regulatory signals required for the priming of MHC class I restricted $CD8^+$ cytotoxic T lymphocytes (CTLs), which are thought to serve as the dominant effector cells mediating tumor killing. Induction of $CD4^+$ responses required for the maximal systemic antitumor immunity by MHC II molecules results in the production of cytokines and interferon γ (INF-γ) that activate eosinophils and macrophages. These two cell types produce superoxide and nitric oxide which in collaboration with CTLs causes the destruction of tumor cells [14, 15]. However, for the activation of MHC II molecules, the conformation itself plays a major role to initiate the whole process of tumor cell killing. Various methods are used to stimulate the peptide-receptive state of MHC II protein by MHC Loading Enhancers (MLEs), small organic catalytic compounds that are simply added to the antigen mixture

[16–21] but all these methods are under consideration due to the stimulation of autoimmune responses [22]. It is safer to use the naturally occurring MHC II molecules by making them more responsive rather than entangling ourselves with the approach of generating large recombinant fusion proteins. In APCs, antigen presentation via MHC II proteins occurs in intracellular endosomal compartments (acidic lysosomal-like vacuole), where peptides are generated and loaded onto class II MHC proteins followed by transport to the surface, and presentation to $CD4^+$ cells. In contrast to this, the mechanism adopted by MLEs relies on the fact that on cell surface the efficacy of antigen loading by MHC II is held up by the lack of empty and accessible MHC II molecules. Either they are already occupied by endogenous peptides or, after loosing their peptide, have converted to a non-receptive state. This instant transformation into the peptide non-receptive state is regarded as a safety-mechanism, preventing the loading of unnecessary self-antigens on the surface. Experiments with fixed cells or MHC expressing cells lacking essential components of the endocytic pathway indicate that MHC II loading can also take place directly on the cell surface. Presentation of immunodominant epitopes in the haemagglutinin (HA) protein of influenza virus and in myelin basic protein (MBP) occurred with the truncation of either one of the α or β cytoplasmic tails that virtually eliminates the need for internalization of HLA-DR molecules, contribute an alternative antigen presentation pathway [23]. Another antigen, delipidated MBP (HP-MBP) also follows the same presentation pathway which is independent of HLA-DM [24]. Furthermore, encephalitogenic MBP is transferred with immense efficiency onto HLA-DR molecules when hydrogen bond donor molecules such as para-chlorphenol (pCP) are present [16]. Specially, immature dendritic cells (DCs) utilize this pathway as they contain a large fraction of empty class II MHC molecules on the cell surface, which may allow the direct capturing of antigens from the extracellular space. The ability of the empty cell-surface class II MHC proteins to bind peptides and present them for the surveillance by $CD4^+$ cells evading intracellular processing can lead to broaden the spectrum of antigens able to be presented by DCs, coherent with their role as protector in the immune system [25, 26]. Small organic compounds (MLEs) can improve antigen loading by switching the MHC II protein from the inactive peptide non-receptive state to the active peptide-receptive state and by triggering the release of ligands with lower affinity [17, 19]. Similarly to HLA-DM, these MLEs stabilize a peptide receptive state followed by accelerated antigen-loading and ligand exchange. By marking the conserved P1-pocket residing within the binding cleft of MHC II molecules, these MLEs are able to stabilize the peptide receptive state, which allows efficient loading of APC with T cell antigens. A series of adamantyl derivatives reported by high-throughput screening [19] is considered as potent allelic-dependent MLEs. After para-chlorophenol (pCP), which induces the peptide-receptive state of MHC II in an allele-independent manner, adamantyl derivatives are the most potent activators of MHC II molecules (1,000–62.5 μM in a dose–dependent manner). HLA-DRs expressing a glycine residue at the dimorphic β86 position results in a striking enhancement of $CD4^+$ cell responses. For this reason, such HLA-DRs are regarded as 'adamantyl-susceptible'. These adamantyl compounds serve to stabilize the conformational requirements of MHC II molecules needed to display the peptide so that recognition and then destruction of tumor cells by an immune cascade is made effective. In addition, adamantyl compounds are also involved in peptide-exchange process by removing low-affinity peptides but not high-affinity ones. Several studies in mouse models have shown that long-term defense required sufficient and persistent $CD4^+$ cell responses which help the effector cells (CTLs) to accomplish their task via the production of several cytokines [1]. It is only possible when MHC molecules remain in their peptide-receptive form. In vitro, the presence of MLEs such as adamantyl derivatives during antigen loading increased the sensitivity of $CD4^+$ cell response for a model antigen by up to two orders of magnitude [19]. Likewise, in vivo activity of adamantyl compounds [27] also reports that this enhancing effect as shown by $CD4^+$ cells is observed when an admantyl compound (AdEtOH) is used as an additive during vaccination with TAA derived from recombinant NY-ESO-1 protein.

At molecular level, experimental confirmation of molecular interactions formed by adamantyl compounds as MLEs with MHC II molecules is not yet defined. It is beneficial to approach these questions by alternative methods. Purification of peptide-free HLA-DRs is more cumbersome than the peptide-loaded HLA-DRs. Conditions required for the crystallization of peptide-free HLA-DR have yet to be determined. Yet, knowledge about MHC II interactions with adamantyl derivatives may lead to better MLEs. This study focuses on the identification of molecular interactions formed by adamantyl compounds with MHC II molecules and the molecular transition of MHC II molecules induced by this series of compounds. Various in silico tools were applied to investigate where the adamantyl compounds bind in the vicinity of Gly/Valβ86 dimorphic MHC II molecules. We also investigated why Valβ86 is not susceptible to adamantyl compounds contrary to what is seen with Glyβ86. Finally, we endeavored to predict what conformational changes occur as a result of binding by adamantyl derivatives.

To address the above-mentioned issues, five cavities are predicted around P1 pocket but only one cavity is preferred

over the others. This selection is based on the size, accessible surface area (ASA) and neighboring amino acid residue environment around the predicted cavities. All six reported adamantyl derivatives were docked into two different allelic variants: PDB IDs—1AQD (Glyβ86), and 1BX2 (Valβ86). All of the generated conformations were then scored and re-ranked to evaluate which of these conformations best complements the protein binding site [28]. Molecular interactions of all 12 docked poses were revealed, including the identification of the best binding pose according to different conditions. Molecular dynamics simulations of peptide-free and peptide-loaded states were carried out on both HLA-DRs allelic variants. To develop a self-consistent model describing the MHC and MLE interactions on a molecular level, the molecular interactions of 3-(1-adamantyl)-5-hydrazidocarbonyl-1H-pyrazole (AdCaPy) inside the predicted cavity of both HLA-DRs allelic variants was analyzed. Our goal in this work was to gain insight into structural changes that may occur in the absence of bound peptide but in the presence of AdCaPy, and if MHC II could adopt a peptide-receptive state.

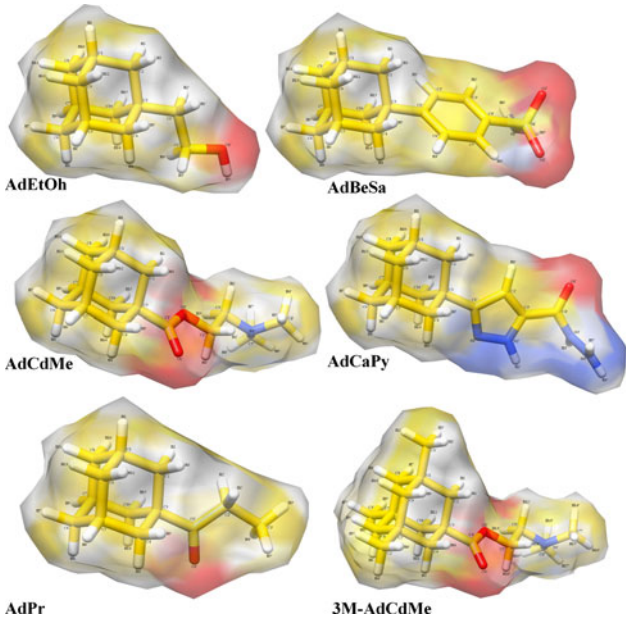

Fig. 1 3D structures of all six adamantyl derivatives represented as stick models along with their electrostatic molecular surfaces. Atom numbering assigned by MVD is used for demonstrating docking interactions (see "Results and Discussion")

Materials and methods

Preparation of adamantyl compounds as MLEs

Six adamantyl derivatives, 2-(1-adamantyl)ethanol (AdEtOH), 3-(1-adamantyl)-5-hydrazidocarbonyl-1H-pyrazole (AdCaPy), 4-(1-adamantyl)benzenesulfonamide (AdBeSA), 1-propionyladamantane (AdPr), 1-[2-(N,N-dimethylamino)-ethoxycarbonyl]adamantane (AdCDME), and 1-[2-(N,N-dimethylamino) ethoxycarbonyl]-3,5,7-trimethyladamantane (3M-AdCDME) [19] (Fig. 1) were selected for docking onto the P1 pocket of two different allelic variants of HLA-DRs—HLA-DRA: DRA*0101, DRB1*0101; PDB ID: 1AQD, and HLA-DR2b: DRA*0101, DRB1*1501; PDB ID: 1BX2). SYBYL® software package (version-7.3, TRIPOS, St. Louis, MO) [29] was used to build three dimensional (3D) structures of six adamantyl derivatives that were subsequently used for docking. Adamantyl derivatives were annotated with their atom types and charged by the Gasteiger-Marselli method [30]. Hydrogen atoms were added and minimization was performed with a convergence criterion of 0.05 kcal/mol Å through the Tripos force field [31] until convergence in the gradient was achieved.

Selection of HLA-DRs

Crystal coordinates of two different allelic variants of HLA-DRs, both of mammalian (*Homo sapiens*) origin were downloaded, from the PDB databank [32]. HLA-DR1 complexed with an endogenous peptide A2 (103–117) (PDB ID: 1AQD) [33] was preferred over 1DLH [34], HLA-DR1 complexed with an influenza virus peptide, haemagglutinin (HA; 306–318) since it has a better overall resolution (2.45 Å) than 1DLH (2.80 Å). 1AQD and 1DLH both belong to the same class of genetic variant and have glycine at their β86 position. Although, instead of extensive conformational variability allowed for bound peptides, the HLA-DR1 protein residues in both PBD structures have almost the same hydrogen bonding pattern against the two completely different peptide sequences. In addition, these peptides also adopt essentially the same bound conformation. Two water molecules were observed in the bottom of the P1 pocket of the HLA-DR1-HA complex, engaging-Thrβ90 and peptide's Tyr308 hydroxyl group to form hydrogen bonds. In the HLADR1-A2 complex, an unexpectedly new orientation of the tryptophan side chain in the P1 pocket cannot provide a hydrogen bond to a water molecule bound to Thrβ90. This results in a non-ordered water molecule which we disregard.

Crystal structure coordinates of two HLA-DR β chains, DRB1*1501 [35] (PDB ID: 1BX2) and DRB5*0101 [36] (PDB ID: 1FV1) are available with the same bound human myelin basic peptide-specific $CD4^+$ cells (MPB; 85–99). 1FVR is an allelic variant that has glycine at its β86 position, in contrast to 1BX2 that has valine at its β86 position constituting the P1 pocket, and since we are interested to explore the specificity that appears to be modulated by a Gly/Val dimorphism, 1BX2 was chosen for further study.

Preparing HLA-DRs molecules for docking

Only α and β polypeptide chains were kept by deleting all their natural peptides and crystallographic water molecules from the structure fles. Proper bond assignments, bond orders, hybridization and charges were calculated by MolegroVirtual Docker software (MVD; version-3.0.0 [37]). Explicit hydrogens were added and their hydrogen bonding patterns were also determined by MVD.

Cavity, detection, selection and optimization

Ours is the first study to report an MLE binding site near the P1 pocket. We carefully evaluated the detected cavity to ensure that it was large enough to accommodate the activator and at the same time satisfy all necessary hydrogen bonding interactions. In order to predict potential binding sites for adamantyl compounds on HLA-DR, a grid-based cavity detection algorithm [37] was employed using a molecular surface (expanded van der Waals) feature. A discrete grid with a resolution of 0.80 Å was generated having a sphere of radius 1.4 Å that was placed at every grid point. A maximum of 16 ray checks was set and a grid point was assumed to be part of a cavity if 12 of these rays hit an inaccessible volume. A maximum of five cavities were detected. For each docking run, selected cavities were further refined by side chain minimization (Nelder-Mead Simplex Minimization Algorithm) via a maximum of steps per residue (10,000) and a maximum number of global steps (10,000).

Docking of adamantyl compounds on HLA-DRs

Docking search algorithms and scoring functions

MVD has two docking search algorithms; MolDock Optimizer and MolDock SE (Simplex Evolution). MolDock Optimizer is the default search algorithm in MVD [38, 39] which is based on an evolutionary algorithm. In MVD version 1.5, an alternative heuristic search algorithm named MolDock SE (simplex evolution) is also implemented. MolDock SE performs better on some complexes where the standard MolDock algorithm fails. Likewise, the two scoring functions; MolDock Score and its grid-based version, MolDock Score [GRID] [40–42] were used for evaluating docking solutions. Exhaustive docking calculations were performed by using both search algorithms along with both scoring functions. Hence, for each adamantyl derivative a total of 20 scores were generated per 5 poses returned from each docking run. The following optimization parameters were used for each search algorithm and scoring function.

Parameters for docking search algorithms

MolDock optimizer

In MVD, the following parameters were used for the guided differential evolution algorithm: number of runs = 10 (by selecting the 'constrain poses to cavity' option), population size = 50, maximum iterations = 2,000, crossover rate = 0.9, and scaling factor = 0.5. The variance-based termination scheme was selected rather than root mean square deviation (RMSD). To ensure the most suitable binding mode in selected binding cavity, pose clustering was employed to obtain multiple binding modes.

MolDock SE

For pose generation, 1,500 maximum iterations were used by selecting a population size of 50. These poses were built incrementally from their rigid root point. The pose generator tests a number of different torsion angles, rotations and translations, evaluates the affected part of the molecule and chooses the value which results in the lowest energy contribution. Generated poses were added to the population if the energy value was below a 100.0 threshold. At each step, at least 10 torsions/translations/rotations were tested and the one giving lowest energy was chosen. If the energy was positive (e.g., because of a clash or an unfavorable electrostatic interaction) an additional 10 positions were tested. If it was still not possible to construct a component which does not clash, a maximum of 10 was additional attempts were performed. Simplex Evolution parameters were set at 300 steps with neighbor distance factor of 1.0.

Parameters for scoring functions

MolDock score

The 'ignore distant atoms' option was used to ignore atoms far away (≥15 Å) from the binding site. Additionally, hydrogen bond directionally was set to check whether hydrogen bonding between potential hydrogen bond donors and acceptors can occur. The binding site on the protein was defined as extending in X, Y and Z directions around the selected cavity with a radius of 15 Å.

MolDock score [GRID]

The MolDock Score [Grid] is identical to the MolDock Score except that hydrogen bond directionality is not taken into account. The grid-based scoring function provides a 4–5 times speed-up by pre-calculating potential-energy

values on an evenly spaced cubic grid (Hydrogen bonding is determined solely on distance and hydrogen bonding capabilities). The potential energy was evaluated by using a tri-linear interpolation among relevant grid points. A grid resolution of 0.80 Å was set to initiate docking process. The rest of the terms in the MolDock Score [Grid] version (i.e., internal ligand energy contributions and constraint penalties) are identical to the standard version of the scoring function.

Taken together, for each compound, the entire docking process was also run in the presence of all crystallographic water molecules. Forty different types of scores for each adamantyl compound were generated providing us the opportunity to select the best binding mode in the most optimal environment. Docking studies were carried out on a single Intel® Xeon® Quad™ core LINUX OS PC equipped with a single user license of MVD.

Molecular dynamics (MD) simulation study

The elucidation of the HLA-DR: DRA, DRB1*0101-endogenous peptide A2 (PDB ID: 1AQD) and DRA, DRB1*1501-MBP (PDB ID: 1BX2) crystal structures has given us the possibility to investigate these systems on an atomic level through computational analysis. The AMBER MD simulation package (version-10) [44] allowed us to explore six solvated systems: MD simulations of 5 ns were run on three different combinations of each PDB file. The peptide and peptide-free form of both HLA-DRs and the HLA-DRs-MLE(AdCaPy) complexes were subjected to MD calculations in a fully, explicitly solvated box using TIP3P [43] water system under periodic boundary conditions (PBC) in the NPT ensemble. The MD simulations were performed using the SANDER module of AMBER installed on a cluster computing facility at University of Karachi consisting of 10 nodes. Each node has an Intel® Xeon® Quad™ core processor running under the openSUSE 11.0 LINUX environment. Table 1 reports the MD processing data based on the simulation times and other necessary information regarding the six different solvated systems.

Preparing HLA-DRs structures for MD simulation study

The apo structures of the proteins were used as starting coordinates for simulations, and the HLA-DRs-MLEs complexes were prepared by deleting all of the crystallographic water molecules and protein chains, except α and β. For HLA-DRs-peptide complexes, chain C (natural peptide) was retained in both PDBs. The apo structure was named and saved as 1aqd_apo and 1bx2_apo while HLA-DR-peptide complexes were named as 1aqd_whole and 1bx2_whole, respectively. The missing hydrogen atoms were added by SYBYL. The protein systems were subjected to 5,000 cycles of steepest descent and 5,000 cycles of conjugate gradient minimization.

Optimization of HLA-DRs-AdCaPy complexes

The AMBER03 force field [44] was used to establish the potentials of HLA-DRs, and the generalized AMBER force field (gaff) [45] was used to establish the potentials of AdCaPy. The complex structures were saved as 1aqd_adcapy and 1bx2_adcapy, respectively.

Molecular dynamics simulation protocol

The following procedure was used to run MD simulation protocol on all six modeled PDB files. To neutralize the overall net charge of each system, Na^+ ions were placed randomly in the simulation box, away from the protein, and then the whole system was immersed in a rectangular box of TIP3P water system. The water box extended 10 Å away from any solute atoms. Before the MD simulations, molecular mechanics minimizations were performed to relax the system using three steps: (1) the water molecules were relaxed by restraining the protein (2,500 cycles of steepest descent and 2,500 cycles of conjugate gradient minimizations); (2) the counter ions (Na^+) were relaxed (2,500 cycles of steepest descent and 2,500 cycles of conjugate gradient minimizations); (3) the whole system was relaxed without any restraints (5,000 cycles of steepest

Table 1 The composition of different solvated systems along with their run time

Solvated systems	Total no. of residues	Total no. of residues atoms	Total no. of water	Total no. of water atoms	Added counterions	Total atoms	CPU time (days)
1aqd_apo	366	5,896	8,655	55,965	17	61,878	7.29
1aqd_whole	380	6,139	8,608	55,824	16	61,979	8.33
1aqd_adcapy	366	5,902	8,654	55,961	17	61,918	8.39
1bx2_apo	371	5,982	8,612	53,574	16	59,572	7.37
1bx2_whole	385	6,216	7,779	53,336	17	59,569	7.99
1bx2_adcapy	371	5,988	7,857	53,571	16	59,613	8.39

descent and 5,000 cycles of conjugate gradient minimizations). In the MD simulations, the long-range electrostatic interactions were calculated using the particle mesh Ewald (PME) summation method [46] and were updated in every 0.5 fs. The SHAKE procedure [47] was utilized to constrain all bonds to hydrogen atoms which allowed for a time step of 2 fs. The system was gradually heated in the NPT ensemble from 0 to 300 K over the course of 40 ps, and then the entire system was allowed to equilibrate at 300 K for an additional 25 ps. During this equilibration process, constant volume periodic boundary condition was applied. An unrestrained equilibration was also done for 5 ps. Langevin dynamics with a collision frequency (γ) of 1 was used and a non bonded cutoff value of 10 Å was set. Then, 5 ns of production MD simulations were performed under normal temperature (300 K). Constant pressure periodic boundary conditions were utilized during the production runs. The PTRAJ module of AMBER package was used for the evaluation of the resulting trajectories. Snapshots from the trajectories were aligned using the backbone atoms and then further analyzed by VMD (version-1.8.6) [48]. CHIMERA (version-1) [49] was also used to visualize the structures obtained after the MD simulations.

Results and discussion

Detection of cavity for docking adamantyl derivatives as MLEs around HLA-DRs P1 Pocket

Generally, the cavities detected by MVD are selected on the basis of their position located close to the dimorphic site, but a closer look reveals why one cavity should be regarded as the best. For each docking run, only one cavity outperforms all other cavities (Fig. 2). Table 2 summarizes the output generated by the cavity detection algorithm of MVD that includes the cavity volume (Å^3), accessible surface area (ASA-Å^2) and neighboring amino acid residues within 10 Å of each cavity. It is readily observed that in both PDB structures, the presence and absence of water did not allow cavity detection algorithm to make any noteworthy discrepancies—that is, the amino acid residues around predicted cavities remains the same, further confirming the basis of selection of these two genetic variant pairs. The average cavity volume for 1AQD and 1BX2 in the presence and absence of water are almost identical (similarities between two the cavities for both MHC molecules were found to be 86.26 and 98.50%, respectively). Despite this, docking was carried out on both states, but for the sake of clarity, all docking results are assumed to be discussed in the absence of water.

Cavity selection for Glyβ86 allelic variant

Out of many, three amino acid residues, two from the α chain, Pro96, Leu92, and one from the β chain, Tyr102 surrounding cavity 1 are involved in the interactions between the α2 and β2 domains, and are crucial for maintaining the structural aspects of HLA-DRA. The volume of cavity 1 is also too large and did not satisfy the hydrogen bonding interactions between any adamantyl derivative and HLA-DR. The valine/glycine dimorphism at position 86 of the β chain of DR exhibited by most DR alleles has been shown to affect peptide binding. The dimorphism is, therefore, likely to influence antigen presentation but also forms the molecular basis for the observed differences in the stability of Glyβ86 and Valβ86

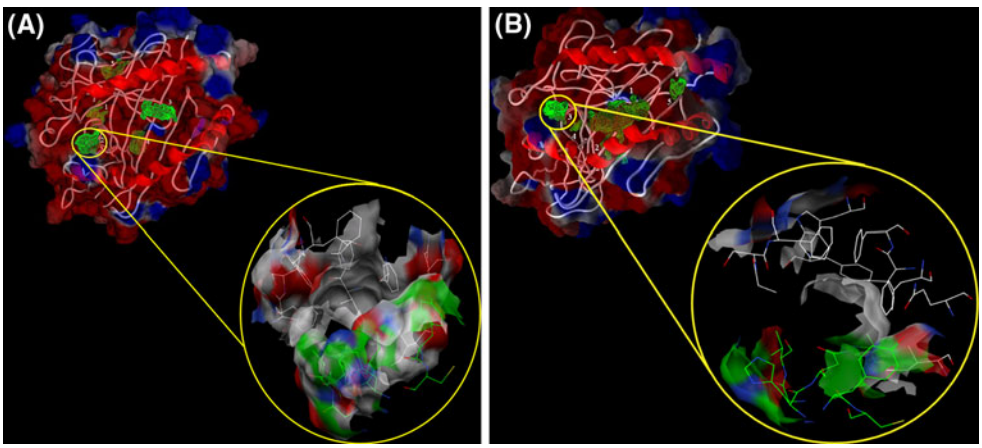

Fig. 2 All cavities as detected by the MVD cavity detect algorithm are shown on HLA-DRs **a** HLA-DRA (PDB ID: 1AQD) and **b** HLA-DR2b (PDB ID: 1BX2). The HLA-DR chains are displayed as backbone with surface representation. The *green meshwork area* indicates the cavity region along with their numbering. The magnified area shows the stick representation of the selected cavity for docking, *white* (α chain) and *green* (β chain)

Table 2 Cavities as detected by MVD cavity detection algorithm

Cavities	Cavity volume (Å^3)	ASA (Å^2)	Neighboring amino acid residues
1AQD (In presence of water)			
Cavity 1	76.28	328.96	Lα92, Tα93, Sα95, Pα96, Vα97, Eα98, Wα178, Fα180, Aspα181
			Yβ102, Sβ104, Vβ116, Sβ118, Lβ158
Cavity 2	**48.64**	**148.48**	**Iα7, Qα9, Fα24, Iα31, Fα32, Wα43, Fα48, Aα52, Sα53, Fα54**
			Yβ78, Cβ79, Nβ82, Yβ83, Gβ84, Vβ85, Gβ86, Fβ89, Tβ90
Cavity 3	38.41	152.32	Gα11, Aα61, Nα62, Aα64, Vα65, Dα65
			Wβ9, Lβ11, Fβ13, Eβ28, Cβ30, Wβ61, Lβ67, Nβ69, Rβ71
Cavity 4	26.62	117.76	Vα6, Iα8, Dα25, Fα26, Dα27, Gα28, Dα29, Lα138, Pα139, Rα140, Eα141, Hα143, Rα146
			Eβ14, Qβ149
Cavity 5	14.33	57.60	Vα65, Aα68, Nα69, Lα70, Eα71, Iα72, Mα73, Rα76
			Wβ9, Cβ30, Sβ37, Lβ53, Gβ54, Pβ56, Dβ57, Aβ58, Yβ60, Wβ61
1AQD (in absence of water)			
Cavity 1	67.58	259.84	Lα92, Tα93, Sα95, Pα96, Vα97, Eα98, Wα178, Fα180, Aspα181
			Yβ102, Sβ104, Vβ116, Sβ118, Lβ158
Cavity 2	**45.05**	**133.12**	**Iα7, Qα9, Fα24, Iα31, Fα32, Wα43, Fα48, Aα52, Sα53, Fα54**
			Yβ78, Cβ79, Nβ82, Yβ83, Gβ84, Vβ85, Gβ86, Fβ89, Tβ90
Cavity 3	32.76	125.44	Gα11, Aα61, Nα62, Aα64, Vα65, Dα65
			Wβ9, Lβ11, Fβ13, Eβ28, Cβ30, Wβ61, Lβ67, Nβ69, Rβ71
Cavity 4	27.13	112.64	Vα6, Iα8, Dα25, Fα26, Dα27, Gα28, Dα29, Lα138, Pα139, Rα140, Eα141, Hα143, Rα146
			Eβ14, Qβ149
Cavity 5	17.92	81.92	Vα65, Aα68, Nα69, Lα70, Eα71, Iα72, Mα73, Rα76
			Wβ9, Cβ30, Sβ37, Lβ53, Gβ54, Pβ56, Dβ57, Aβ58, Yβ60, Wβ61
1BX2 (in presence of water)			
Cavity 1	72.19	250.28	Qα9, Nα62
			Pβ11, Rβ13, Fβ26, Dβ28, Yβ30, Fβ40, Fβ47, Wβ61, Dβ66, Iβ67, Lβ68, Eβ69, Qβ70, Aβ71, Aβ74, Yβ78
Cavity 2	48.12	175.36	Eα3, Vα6, Iα8, Dα25, Fα26, Dα27, Gα28, Pα139, Rα140, Eα141, Rα146
			Kβ12, Eβ14, Hβ16, Rβ29
Cavity 3	**34.81**	**110.08**	**Iα7, Qα9, Fα24, Iα31, Fα32, Wα43, Fα48, Aα52, Sα53, Fα54**
			Yβ78, Cβ79, Hβ81, Nβ82, Gβ84, Vβ85, Vβ86, Tβ90
Cavity 4	24.06	98.56	Kα92, Tα93, Nα94, Sα95, Pα96, Vα97
			Yβ102, Sβ118, Sβ120, Tβ145, Iβ148, Qβ156, Lβ158
Cavity 5	19.96	92.16	Nα69, Iα72, Mα73, Rα76
			Wβ9, Yβ30, Sβ37, Vβ38, Nβ57, Yβ60, Wβ61
1BX2 (in absence of water)			
Cavity 1	73.72	244.48	Qα9, Nα62
			Pβ11, Rβ13, Fβ26, Dβ28, Yβ30, Fβ40, Fβ47, Wβ61, Dβ66, Iβ67, Lβ68, Eβ69, Qβ70, Aβ71, Aβ74, Yβ78
Cavity 2	40.96	162.56	Eα3, Vα6, Iα8, Dα25, Fα26, Dα27, Gα28, Pα139, Rα140, Eα141, Rα146
			Kβ12, Eβ14, Hβ16, Rβ29
Cavity 3	**35.84**	**115.2**	**Iα7, Qα9, Fα24, Iα31, Fα32, Wα43, Fα48, Aα52, Sα53, Fα54**
			Yβ78, Cβ79, Hβ81, Nβ82, Gβ84, Vβ85, Vβ86, Tβ90
Cavity 4	29.69	133.96	Kα92, Tα93, Nα94, Sα95, Pα96, Vα97
			Yβ102, Sβ118, Sβ120, Tβ145, Iβ148, Qβ156, Lβ158
Cavity 5	20.48	76.80	Nα69, Iα72, Mα73, Rα76
			Wβ9, Yβ30, Sβ37, Vβ38, Nβ57, Yβ60, Wβ61

Cavities in bold are selected for docking studies

containing HLA-DRs, for example, the substitution of glycine by valine shifts the preference towards smaller side chains. Taken together, these results suggest that the natural polymorphism at β86 might be a molecular switch that finely tunes the complexity of the peptide collection presented by DR molecules. Cavity 2 is the most hydrophobic pocket of all as detected by MVD. Besides other amino acid residues, this cavity has one tryptophan, two isoleucine, two tyrosine and five phenylalanine residues making it a preferable binding site for a hydrophobic moiety, in this case, the hydrophobic core of adamantyl derivatives. Cavity 2 has allelic dimorphism as it contained glycine at its β86 position that appears to modulate the specificity towards MLEs, e.g., adamantyl derivatives. The cavity volume is also in range of the adamantyl derivative to be docked. According to these facts, cavity 2 is selected for docking of all adamantyl derivatives to 1AQD (Fig. 2a). Cavity 3 was also considered for docking adamantyl derivatives since it is located close to cavity 2 however most of the residues that comprise this cavity has P6 pocket residues, Glu11, Asn62, Val65 and Asp66 form the α chain while Leu11 and Phe13 from the β chain. Trpα71 from P7 pocket is also detected as part of cavity 3. The involvement of amino acid residues with their main chain and side chain contacts to the anchoring residues of peptides did not allow much opportunity for hydrogen bonding interactions. Residues from the peptide-binding domain ($\alpha 1\beta 1$) involved in interactions with the immunoglobulin-like (Ig-like) domains ($\alpha 2$ or $\beta 2$) are detected as elements of cavity 4. A region of α chain (Phe26–31) is critically engaged with the Ig-like domain fulfilling all of its hydrogen bonding interactions. Only two residues from the β chain are predicted as part of this cavity. Presence of Valα65 makes it selectable over pocket 5. In the HA peptide, Thr (+6) binds in pocket 6, displacing Asnα62, Valα65 and Aspα66 by dislocating the bound water molecule [35]. Threonine is not a preferential residue at position 6, and substitution of the HA peptide threonine by alanine increased binding affinity approximately by threefold [50]. Comparison of the HA and A2 peptide complexes in this region suggests that the threonine side chain makes unfavorable polar–nonpolar contacts between its Cγ atom and polar residues near the water site, and between its side chain hydroxyl group and Valα65. Due to the presence of an ordered bound water molecule in this cavity, this cavity was not selected.

Cavity selection for Valβ86 allelic variant

Due to the close allelic variant, 1BX2 has nearly the same amino acid residues around the 5 cavities (Table 2). In the crystal structure of HLA-DR2b-MBP, valine of the MBP occupies the hydrophobic P1 pocket. HLA-DR2b has allelic Vβ86 at the base of the P1 pocket which results in a smaller pocket, in contrast to the situation observed for HLA-DR1 and HLA-DR4 (Gly at β86). A hydrophobic pocket identical to that reported for HLA-DR3 [51] is present but only with the characteristic nature of accommodating small substances. Cavity 3 is selected for docking of adamantyl derivatives (Fig. 2b) since it is the most hydrophobic cavity of all, and contains the allelic valine residue.

Docking of adamantyl derivatives to HLA-DRs allelic variants

All six adamantyl compounds were docked against selected cavity in both HLA-DRs. Due to the paucity of information concerning MHC-MLE interactions, two search algorithms were used alternatively with two scoring functions to increase the computational rigor. This exercise provides for each adamantyl derivative a collecction of scores resulting in different conformations and binding poses. The search algorithm MolDock SE, in combination with the MolDock scoring function produced the best docking results, irrespective of which adamantyl compound that was docked onto which HLA-DR allelic variant. In order to justify the selection of most appropriate HLA-DRs-adamantyl derivative complex, more than one criterion was used to decide which docking solution was more optimal, e.g., least MolDock score (most cases), lowest energy conformation of the adamantyl compound (some cases), and most favorable binding pose having maximum interactions (rare cases). The presence of crystallographic water did not alter the docking solutions. Table 3 shows only the best energetic calculations for each docking run.

Analysis of interactions and binding poses

The atoms of adamantyl derivatives and amino acid residues of 1AQD and 1BX2 that participated in the protein–ligand interactions are presented in Table 4. Docking results reveal a well correlated experimental conclusion. With the exception of AdCdMe and 3M-AdCdMe that MVD ranks with higher MolDock scores, remaining adamantyl compounds are ranked on the basis of their ability to activate HLA-DRs. The docking outcomes are also consistent with the consideration of susceptibility of dimorphic β86 position, further augmenting the preferred cavity selection. Due to Glyβ86, AdCdMe and 3M-AdCdMe have more favorable MolDock scores as compared to its Valβ86 counterpart. Hydrophobic nature of the selected pocket additionally provide suitable environment for these two much bulkier adamantyl derivatives. AdCaPy did not accommodate well in the binding cavity of HLA-DR.

Table 3 Energetic calculations by MVD of different docking parameters

Name of adamantyl derivatives	MolDock score	E-inter (protein–ligand)	H-bond (kcal/mol)	LE1	LE3	Pose energy (kcal/mol)	Rerank score (kcal/mol)
1AQD (in presence of water)							
AdEtOh	−68.50	−87.46	−2.50	−5.27	−4.58	−68.50	−59.51
AdCaPy	−107.76	−125.60	−2.25	−5.67	−4.92	−107.75	−93.52
AdBeSa	−84.86	−109.72	−6.70	−4.24	−1.05	−84.86	−20.91
AdPr	−61.87	20.91	0	−4.42	−4.25	−60.55	−59.44
AdCDME	−91.69	−118.03	−3.04	−5.09	−4.21	−91.67	−75.73
3M-AdCDME	−103.16	−122.50	−2.23	−4.91	−0.99	−103.16	−20.76
1AQD (in absence of water)							
AdEtOh	−69.17	−87.47	−2.50	−5.32	−4.54	−69.17	−59.07
AdCaPy	−105.32	−126.69	−5.53	−5.54	−4.96	−105.32	−94.33
AdBeSa	−84.94	−109.43	−6.54	−4.25	−1.28	−84.93	−25.62
AdPr	−62.47	−85.28	0	−4.46	−4.00	−62.47	−55.98
AdCDME	−91.17	−118.14	−2.50	−5.06	−4.10	−91.17	−73.79
3M-AdCDME	−102.99	−122.40	−2.17	−4.90	−1.03	−102.99	−21.69
1BX2 (in presence of water)							
AdEtOh	−59.06	−77.40	0	−4.54	−4.30	−58.73	−55.85
AdCaPy	103.59	85.87	7.55	5.45	44.33	−73.98	842.23
AdBeSa	−69.26	−94.94	−4.46	−3.46	−2.40	−68.20	−48.09
AdPr	−61.17	−82.88	0	−4.37	−3.99	−61.17	−55.89
AdCDME	−77.21	−103.28	−2.50	−4.29	−1.68	−73.86	−30.31
3M-AdCDME	−83.41	−97.01	−2.24	−3.97	−2.75	−81.78	−57.65
1BX2 (in absence of water)							
AdEtOh	−59.04	−77.39	0	−4.54	−4.30	−58.67	−55.88
AdCaPy	51.90	34.16	−3.24	2.73	33.62	−73.95	638.79
AdBeSa	−68.40	−92.93	−4.85	−3.42	−1.74	−67.79	−34.77
AdPr	−61.26	−83.06	0	−4.37	−3.98	−61.25	−55.66
AdCDME	−73.14	−95.92	−2.49	−4.06	−2.66	−72.22	−47.915
3M-AdCDME	−83.25	−96.73	−2.28	−3.96	−2.58	−81.64	−54.22

2-(1-adamantyl ethanol (AdEtOH)

The oxygen atom (O1′) of the hydroxyl group of AdEtOH mediated a hydrogen bond with the Oγ of Thrβ90 of 1AQD with a MolDock score of −69.17 at a distance of 2.86 Å (Fig. 3a). The energy value of this hydrogen bond was −2.00. Residues from the β chain, Valβ85 and Pheβ89 provide a hydrophobic environment for the core of the adamantine group. Pheα26 43 kcal/mol. Six amino acid residues from the α chain, Ile7, Phe26, Ile31, Phe32, Trp43 and Ala52 and two amino acid is not predicted to be a part of the selected cavity, although its Cε1 and Cδ1atoms are located 3.67 and 3.30 Å, respectively, from the O1′ atom of AdEtOH further increasing the hydrophobic environment. While, in case of 1BX2, none of the atoms of AdEtOH are involved in hydrogen bonding interactions. The calculated MolDock score of this solution is −59.04 (Fig. 3f). Two other poses of AdEtOH formed hydrogen bonding interactions with Asnβ82 and Hisβ81, respectively. However, these two poses were not selected because of their low MolDock scores in several docking runs, and more importantly their steric clash with the allelic Valβ86 position. This type of clash causes the side chain of AdEtOH to rotate in an unusual manner, further increasing the internal energy of the pose (up to 21.67 kcal/mol).

3-(1-adamantyl)-5-hydrazidocarbonyl-1H-pyrazole (AdCaPy)

AdCaPy formed six hydrogen bonds with 1AQD having a calculated MolDock score of −105.32. The hydrazidocarbonyl oxygen atom (O1′) of AdCaPy formed a hydrogen bond with the Oγ atom of Thrβ90 at a distance of 3.06 Å. The nitrogen of the amide group of hydrazidocarbonyl (N3′) of AdCaPy mediated a weak hydrogen bonding interaction with the Oγ atom of Thrβ90 at a distance of

Table 4 Hydrogen bonding interactions of selected adamantyl derivatives with the indicated allelic HLA-DRs

Adamantyl derivatives	Interactions	1AQD atom	Adamantyl atom	Distance (Å)	**Glycine vs. Adamantyl	
					Gly NH (Å)	Gly O (Å)
(a) 1AQD						
AdEtOH	1	Oγ Thrβ90	O1′	2.86	4.90	4.60
AdCAPY	6	Oγ Thrβ90	O1′	3.06	4.23	5.76
		Oγ Thrβ90	N3′	3.59	3.72	4.33
		Oγ Thrβ90	N4′	3.28	4.68	4.74
		Carbonyl O Tyrβ83	N3′	3.28	3.72	4.33
		Carbonyl O Tyrβ83	N4′	3.50	4.68	4.74
		Carbonyl O Asnβ82	N3′	3.02	3.72	4.74
AdBeSA	4	Oγ Thrβ90	N1′	3.09	3.80	4.00
		Carbonyl O Asnβ82	N1′	3.47	3.80	4.00
		Carbonyl O Tyrβ83	N1′	3.44	3.50	4.00
		Oγ Thrβ90	O1′	2.59	5.30	4.20
AdCDME	1	Oγ Thrβ90	N1′	2.98	4.40	4.30
3M-AdCDME	1	Oγ Thrβ90	N1′	3.16	4.20	4.10
Adamantyl derivatives	Interactions	1BX2 atom	Adamantyl atom	Distance (Å)	**Valine vs. Adamantyl	
					Val NH (Å)	Val O (Å)
(b) 1BX2						
AdCaPy	6	Nδ2 Asnβ82	N1′	3.13	5.00	10.90
		OH Tyrβ78	N2′	3.57	9.10	11.30
		Nδ2 Asnβ82	N2′	2.83	9.10	11.30
		Nδ2 Asnβ82	O1′	2.61	9.70	12.10
		OH Tyrβ78	O1′	3.36	9.70	12.10
		Carbonyl O Ileα7	N4′	3.18	10.00	11.70
AdBeSA	2	Nε2 Glnα9	O2′	3.13	14.10	16.70
		Oε1 Glnα9	N1′	3.09	13.20	16.00
AdCDME	1	Peptide N Glnα55	N1′	3.09	12.10	14.90
3M-AdCDME	1	Nδ2 Asnβ82	O2′	3.14	9.50	12.40

* AdPr is not included since it has no interactions in either case; the same is true for AdEtOh in 1BX2

** The last two columns show the distances between the interacting adamantyl atom and the dimorphic amino acid residue (peptide amine and carbonyl oxygen)

3.59 Å. The same nitrogen atom of AdCaPy is also involved in a hydrogen bonding interaction with the carbonyl O atoms of Tyrβ83 and Asnβ82 at distances of 3.28 and 3.02 Å, respectively. The nitrogen atom of the amine group of hydrazidocarbonyl (N4′) of AdCaPy formed a hydrogen bond with the Oγ atom Thrβ90 having a distance of 3.28 Å. The same nitrogen atom of AdCaPy behaves as a hydrogen bond donor to the carbonyl O atom of Tyrβ83 with a distance of 3.50 Å. The presence of arene–cation interaction between the aromatic π-electron of Tyrβ83 and the N3′ atom of AdCaPy is indispensable to accommodate the derivative in the vicinity of the predicted cavity (Fig. 3b). There is another pose of AdCaPy which has the lowest MolDock score (−107.76) but it has three problems which caused it to be excluded. First, the overall hydrogen bonding energy of this pose is high (−2.23 kcal/mol) as compared to that made by the selected pose (−5.5 kcal/mol). Second, the C–C torsion between C3 and C1′ of this pose shifted the pyrazole ring to the other side which is responsible not only for changes in the energetics of the pose but also the side chain environment is not able to accommodate the ring structure on that face. The selected pose also has a lower re-rank MolDock score (Fig. 4).

The 1BX2-AdCaPy complex formed six hydrogen bonds and had a MolDock score of 51.90. The pyrazole nitrogen atom (N1′) of AdCaPy interacted with the Nδ2 of Asnβ82 through a hydrogen bond at a distance of 3.14 Å. The amide nitrogen atom (N2′) of the pyrazole ring interacted with the Oη atom of Tyrβ78 and the Nδ2 atom of Asnβ82 through hydrogen bonds with distances of 3.57 and

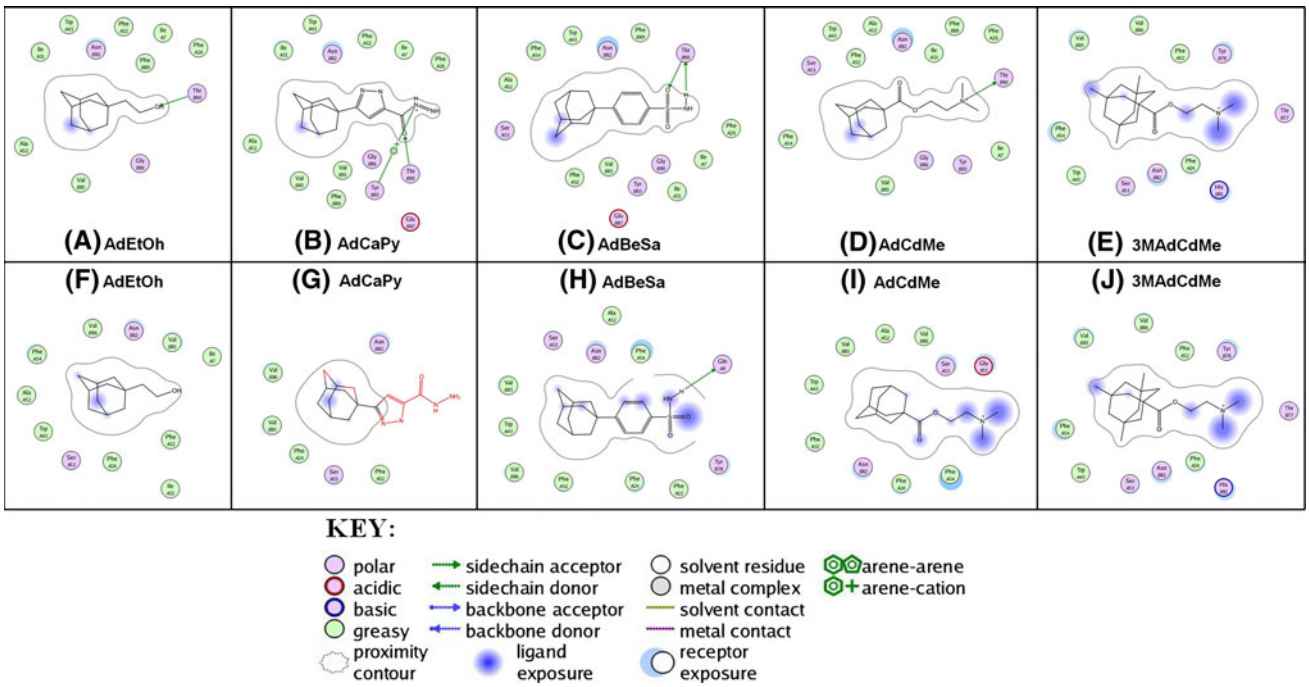

Fig. 3 Binding orientations and hydrogen bonding interactions of adamantyl derivatives with HLA-DR (1*1010-PDB ID: 1AQD); *upper panel* (**a**–**e**), and with HLA-DRB (1*1501—PBD ID: 1BX2); *lower panel* (**f**–**j**). The binding site residues are colored by their nature, with hydrophobic residues in *green*, polar residues in *purple* and charged residues highlighted with *bold* contours. The figure was generated using the LigX application in MOE (Chemical Computing Group, Montreal, Canada)

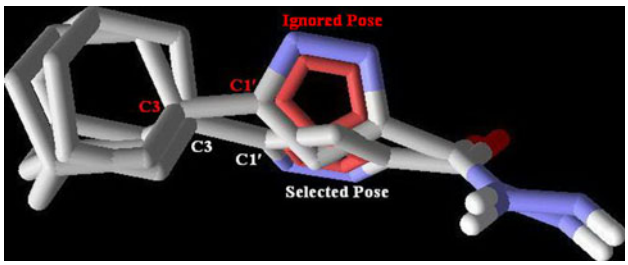

Fig. 4 Two different conformations of AdCaPy in cavity 2 of 1AQD. Observe the change in C–C torsion occur between C3 and C1′ of selected and ignored poses

2.83 Å, respectively. The oxygen atom (O1′) of the hydrazidocarbonyl group of AdCaPy behaves as a hydrogen bond acceptor for the amide nitrogen atom (N) of Asnβ82 and the Oη atom of Tyrβ78 at distances of 2.61 and 3.36 Å, respectively. The amine nitrogen (N4′) of hydrazidocarbonyl of AdCaPy interacted with the carbonyl oxygen atom (O) of Ileα7 via a hydrogen bond of 3.18 Å (Fig. 3g). Due to these interactions, AdCaPy remained outside the cavity since the Cγ1 and Cγ2 atoms of Valβ86 did not provide enough space to accommodate this ligand. The most notable observation of AdCaPy to the docking study against 1BX2 is the positive MolDock scores, irrespective of the search algorithm or scoring function. Due to the presence of Valβ86, the depth of the P1 pocket is restricted [5, 52] such that the Valβ86 pocket can bind only small aliphatic anchor side chains (Ile, Leu, Val, and Met), whereas the deeper Glyβ86-containing pockets also accommodate larger aromatic residues (Phe, Tyr, and Trp). While in case of 1AQD, the calculated MolDock scores are very low confirming the experimental adamantyl susceptibility and correlation of AdCaPy activity with the Glyβ86 allelic variant but the MolDock scores observed for 1BX2 exhibit very high scoring values. These high values suggested that the AdCaPy did not accommodate itself within the small cavity of 1BX2 and most of its side chain remained outside. Through visual inspection of the binding mode of AdCaPy in 1AQD, it is clear that the substitution of AdCaPy at C3 allows the derivative to maintain itself within the selected cavity through hydrogen bonding interactions. There is sufficient room within the cavity to anchor this sort of substitution. In contrast, AdCaPy did not enter into the cavity of 1BX2. The occupation by the side chain of Valβ86 blocks AdCaPy in such a way that the adamantane group lies almost at the same place but is rotated in such a way as to place its bulky substituent outside of the cavity. This may have been the result of MVD docking software while it attempted to satisfy its hydrogen bonding interaction parameter (see Table 4), however, the overall contribution by the remaining parameters made the MolDock score values very high.

4-(1-adamantyl)benzenesulfonamide (AdBeSA)

The AdBeSA formed four hydrogen bonds with 1AQD resulting in a MolDock score of −84.93. The amine nitrogen atom (N1′) of AdBeSA formed a hydrogen bond with Oγ of Thrβ90 at a distance of 3.09 Å. The same nitrogen atom acted as hydrogen donor to the carbonyl oxygen atom of Aspβ82 with a distance of 3.47 Å. The carbonyl O atom of Tyrβ83, at a distance of 3.44 Å, forms a hydrogen bonding interaction with the already engaged amine nitrogen atom. The sulfone oxygen (O2′) of AdBeSA formed a hydrogen bond with Oγ of Thrβ90 at a distance of 2.59 Å (Fig. 3c). In the case of 1BX2, AdBeSA formed two hydrogen bonds with an α chain residue having a MolDock score of −68.40. The sulfone oxygen atom (O2′) of AdBeSA formed a hydrogen bond with Nε2 of Glnα9 at a distance of 3.13 Å. The amine nitrogen atom (N1′) of AdBeSA formed a hydrogen bond with Oε1 of Glnα9 at a distance of 3.09 Å (Fig. 3h).

1-[2-(N,N-dimethylamino)-ethoxycarbonyl]adamantane (AdCDME)

AdCDME formed only one hydrogen bond with 1AQD resulting in a MolDock score of −91.17. The amine nitrogen atom (N1′) of AdCDME formed a hydrogen bond with the Oγ atom of Thrβ90 at a distance of 2.98 Å (Fig. 3d). AdCDME also formed one hydrogen bond when docked into 1BX2, having a MolDock score of −73.14. The amine nitrogen atom (N1′) of AdCDME formed a hydrogen bond with the backbone amide nitrogen atom (N) of Glnα55 with a distance of 3.09 Å (Fig. 3i).

1-[2-(N,N-dimethylamino)ethoxycarbonyl]-3,5,7-trimethyladamantane (3MAdCDME)

3M-AdCDME formed a hydrogen bond with 1AQD with a MolDock score of −102.98. The amine nitrogen atom (N1′) of 3M-AdCDME formed a hydrogen bond with the Oγ atom of Thrβ90 with a distance of 3.16 Å (Fig. 3e). Similarly, 3M-AdCDME formed one hydrogen bond when docked into the binding cavity of 1BX2. The observed MolDock score was −83.25. The ester oxygen atom (O2′) of 3M-AdCDME formed a hydrogen bond with the amide nitrogen atom (Nδ2) of Aspβ82 at a distance of 3.14 Å (Fig. 3j).

Allelicβ86 position in adamantyl susceptibility

Falk et al. [19] reported that adamantyl compounds activate Class II MHC molecules in an allele-dependent manner. Experimentally, they proved that the allelic variations in fact suggested a correlation of susceptibility with a well known dimorphism at position 86 of the β chain [19]. All MHC molecules susceptible to adamantyl compounds expresses glycine at this position, while DRB1*1501, the only non-susceptible molecule identified so far, expressed valine at β86. The same susceptibility and correlation are further confirmed by the docking of adamantyl compounds to the selected HLA-DRs allelic pair. In addition to this, it is critical to gain an accurate molecular view of the interactions and mechanisms that regulate the formation and persistence of peptide-MHC complexes. In order to obtain a detailed understanding of how Glyβ86 is involved in the adamantyl susceptibility, we evaluated the relative energetic contributions of hydrogen bonding interactions within adamantyl-MHC complexes (Table 3).

The protein–ligand energy for the 1AQD-AdEtOh complex is −87.47, and for 1BX2 is −77.390. Likewise, the pose energies for 1AQD and 1BX2 are −69.17 and −58.67, respectively. In both cases, the energies for 1AQD are less than for 1BX2. Moreover, AdEtOH forms only one hydrogen bond with Thrβ90 in the P1 pocket of 1AQD. No hydrogen bonding pattern is observed in 1BX2. In fact, the side chain of AdEtOH is short and is pointed towards the binding groove of P1 pocket of 1AQD and1BX2, but due to the presence of Valβ86 and to prevent a steric clash from the side chain of the allelic Valβ86, AdEtOh shifted slightly away from the Thrβ90 resulting in loss of hydrogen bonding interactions. According to this analysis, it can be hypothesized that AdEtOH is preferably occupying the P1 pocket of 1AQD more exclusively than 1BX2. These inspections support the previously shown experimental results which implicated that adamantyl compounds exhibit MLE activity only for a subset of HLA-DR molecules [19].

Analysis of docked AdCaPy into the selected HLA-DRs allelic pair revealed protein–ligand energy for 1AQD is −124.63, which is much more favorable than that for 1BX2 which is 34.16. Further analysis revealed that AdCaPy did not dock well against 1BX2 due to steric hindrance as exhibited by the very high/positive binding energy.

The AdBeSA docking results revealed that the energies of protein–ligand complexes for 1AQD and 1BX2 are −109.44 and −92.93, respectively. Four hydrogen bonds are formed between AdBeSA and 1AQD. However, the amino acid residues of 1AQD contributing to hydrogen bonding interactions are from the P1 pocket with the exception of Tyrosine β83. While in the case of 1BX2, only two hydrogen bonds are formed with Glnα9 which is a residue in the P4 pocket. AdBeSA could not be accommodated in either HLA-DR. Examination of the AdCDME and 3M-AdCDME docking poses revealed that their side chains projected outward from the P1 binding site. This was caused by the presence of Valβ86 which restricts the depth of the P1 pocket. AdCDME side chain formed a

hydrogen bonding interaction with an amino acid residue that is not a part of cavity 2 (Glnα55). 3M-AdCDME bends at O1′ in an unusual manner causing favorable hydrophobic interactions with the adjacent amino acid residues. These hydrophobic interactions contributed to a lower internal energy of the pose. However, Glyβ86 accommodates the side chains of AdCDME and 3M-AdCDME fairly well.

Asnβ82, Tyrβ83 and Thrβ90 exhibit significant hydrogen bonding interactions in 1AQD (Table 4) While in case of 1BX2, the amino acid residues of other pockets are also involved, such as Glnα9 and Tyrβ78 of the P4 pocket. In addition, Gluα55, the amino acid residue that is not detected as part of any cavity, had a hydrogen bonding interaction with AdCdMe. Overall, the adamantyl compounds can be easily accommodated in the large and mostly hydrophobic P1 pocket of 1AQD. Conversely, Valβ86 in the P1 pocket of 1BX2 is not spacious enough to accommodate the adamantyl compounds, therefore, residues of other pockets contributed hydrogen bonding interactions. The distances from the allelicβ86 position are summarized in Table 4 which further demonstrates the poor accommodation of each pose with respect to the P1 cavity. These docking results substantially support the reported experimental observations.

Molecular dynamics (MD) simulations

MD simulations were carried out in an explicitly solvated system employing periodic boundary conditions in an NPT ensemble. In this study, MD simulations have been used to gain insight into the conformational changes adopted by the HLA-DR β86 allelic pair in the presence of adamantyl derivatives which are known to act as MLEs. AdCaPy was chosen for simulation with 1AQD and1BX2 because of its most favorable protein–ligand binding energy and MolDock score for 1AQD, but very high total protein–ligand energy and MolDock score values for 1BX2. The selection of this adamantyl derivate gave us a clear observation about the impact of the dimorphic residue on susceptibility to adamantyl compounds.

Equilibration properties of the systems

In order to analyze the stability and dynamical properties of the simulated systems, different physical parameters such as total energy (including kinetic energy and potential energy), density, temperature, and pressure etc., are monitored continuously to ensure the stability of the complex. Convergence of all such physical properties is necessary to ensure the physical reliability of the system. If the equilibration properties oscillate around an acceptable value, it is inferred that the system has converged to a metastable state. All plots were drawn using XMGRACE [53].

Analysis of potential energies of all simulated systems

The potential energy of the 1aqd_apo system remains constant during simulation run time. While the potential energy of 1aqd_whole system slowly decreased until 1,000 ps but it became constant during the reminder of the simulation. In the 1aqd_adcapy system, the potential energy decreased significantly until 800 ps but became constant after 5 ns of simulation time (Fig. 5; upper panel). The potential energy profile of the 1bx2_apo system slowly decreased during first 500 ps, and then remained unchanged through the remaining 4,500 ps. Similarly, the potential energy of 1bx2_whole system decreased constantly from the beginning until 1,000 ps. Afterward, it remained constant until the end of the simulation. The potential energy of the 1bx2_adcapy system decreased considerably during first 300 ps. Subsequently, it remained constant until the end of the simulation run time (Fig. 5; lower panel).

Analysis of root mean square deviation (RMSD) of all simulated systems

The simulated RMSDs of the backbone atoms of both proteins also provided information about the structural

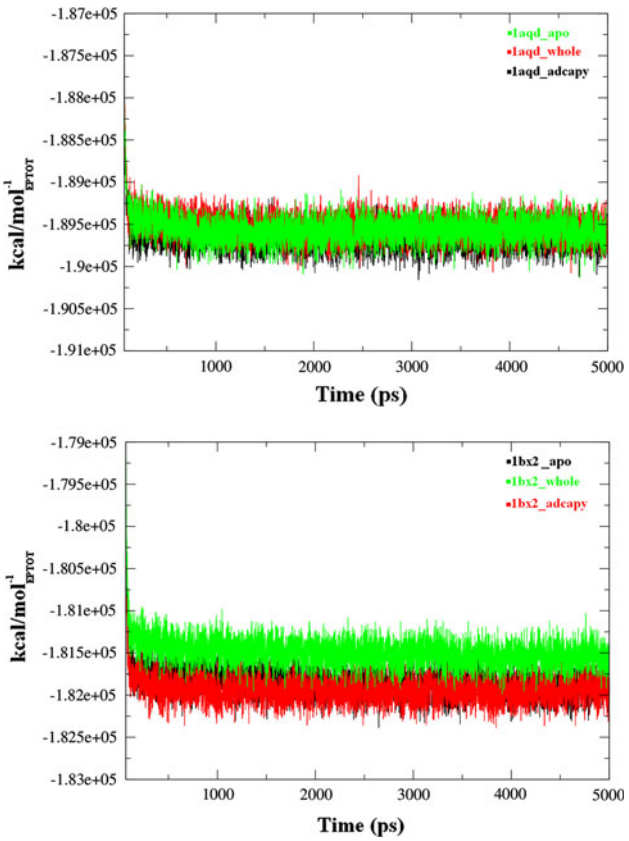

Fig. 5 Potential energies vs. time plot of production runs of: 1aqd systems (upper panel); 1bx2 systems (*lower panel*)

equilibration of the system and to what extent the systems changed relative to their initial structures. The PTRAJ module of the AMBER was used to calculate the overall RMSD of the backbone atoms of each simulated system. In the beginning, the RMSD of the 1aqd_apo system increased more than 2.50 Å until 1,250 ps, and then decreased below 1.50 Å approximately at 3,000 ps. After 3,000 ps, it remains fluctuated till the end of simulation run time. In case of the 1aqd_whole system, the RMSD value slightly increased to 2.00 Å up to 1,000 ps, and then it remains fluctuated over 4,000 ps, after that it become stabilizes. The RMSD plot shows that 1aqd_adcapy system increases significantly with RMSD value of 2.25 Å up to 2,500 ps, then diminished around 3,000 ps. Afterwards, at the end of whole simulation run, the system fluctuates at low RMSD values (Fig. 6; upper panel). It is concluded that the 1aqd_apo system shows the highest range of RMSD values as compared to its respective systems.

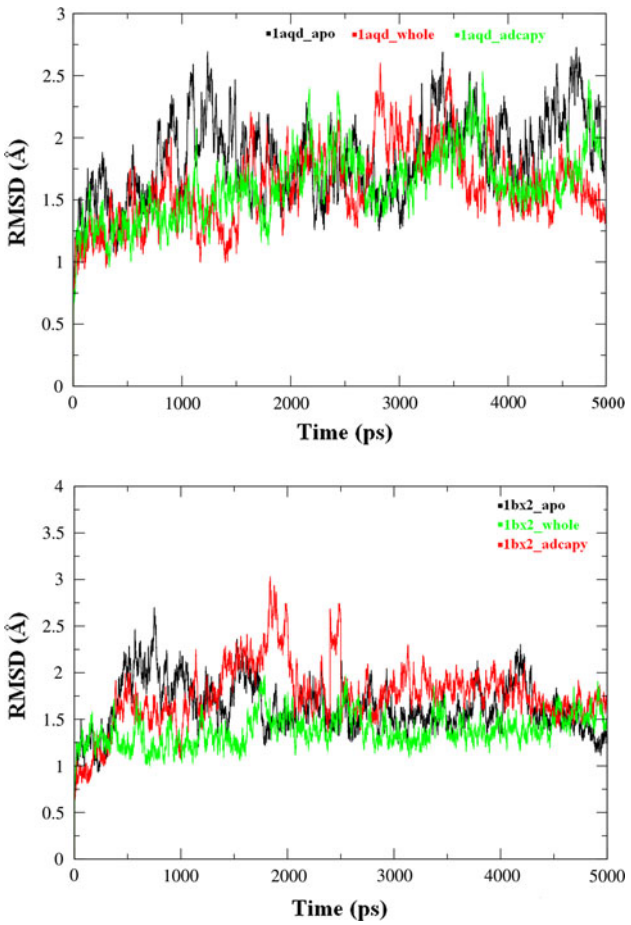

Fig. 6 RMSD values of polypeptide backbone (Cα, C, and N atoms) as a function of time in the production runs for: 1aqd systems (*upper panel*); 1bx2 systems (*lower panel*). *Green curve* (HLA-DRs with AdCaPy systems) indicates almost same polypeptide backbone deviation as that of *red curve* (HLA-DRs with peptide-loaded systems)

However, the RMSD for 1bx2_apo system also increases more than 2.50 Å during the simulation time from 0 to 700 ps, and then it declines to a value of 1.50 Å until 2,000 ps. Afterwards, the RMSD did not change throughout the simulation run. By analyzing the RMSD plots of both apo HLA-DRs allelic variant that shows the rapid significant increase in the beginning followed by sharp decrease clearly demonstrate that major structural changes that may have been taken place during the whole simulation run time eventually convert the peptide-receptive apo form to its peptide non-receptive apo form. The RMSD plot for 1bx2_whole system shows that RMSD stabilizes from the beginning at value of 1.25 Å until 1,500 ps followed by a significant increase to 2.00 Å until 1,800 ps, later it becomes stable all over the whole run time. In 1bx2_adcapy system, rapid increase in the RMSD values is seen over the first 500 ps. Stabilization of RMSD (1.75 Å) is achieved during the simulation time from 500 to 1,000 ps. From 1,000 to 2,000 ps, significant increase to 3.00 Å took place. In fact, it is the time when the interaction of AdCaPy as MLE clashes with the side chain of allelic valineβ86 residue. This steric hindrance renders the system towards more fluctuation until 2,500 ps. It can be hypothesized that after 3,000 ps when AdCaPy accommodates itself outside cavity 2, RMSD becomes stable until the end (Fig. 6; lower panel). The RMSD patterns as adopted by the whole and adcapy HLA-DR Glyβ86 allelic variant systems is almost the same in view of the fact that AdCaPy in Glyβ86 environment provides such suitable interactions that set off this allelic variant to be in the peptide-receptive state. But the whole and adcapy HLA-DR Valβ86 allelic variant systems have differences in their RMSD plots indicating the drastic role of Valβ86 in not providing the appropriate space for the adjustment of AdCaPy as MLE. Large changes in the RMSD values are observed for 1bx2_adcapy system over the 1,500–2,000 ps that reach approximately 3.00 Å to convert itself from the peptide-receptive state to peptide non-receptive state.

Flexibility of binding grooves of HLA-DRs in three different states

Visual analysis of the fluctuations was performed by extracting an average PDB file from the trajectories of each simulated system and then aligning them to determine mean RMSD ($RMSD_{avg}$) values. The systems with the lowest fluctuations are 1aqd_whole and 1bx2_whole with relative $RMSD_{avg}$ values of 0.91 and 0.89 Å, respectively. The β-pleated sheets that form the floors of the peptide site and flanking helices that guard the same site from top and below face remain stable due to the peptide ligands which keep MHC II in its open state (Figs. 7b, 8b). Additionally, in the peptide-bound states the β_{1-1} (β56–65 corresponds to

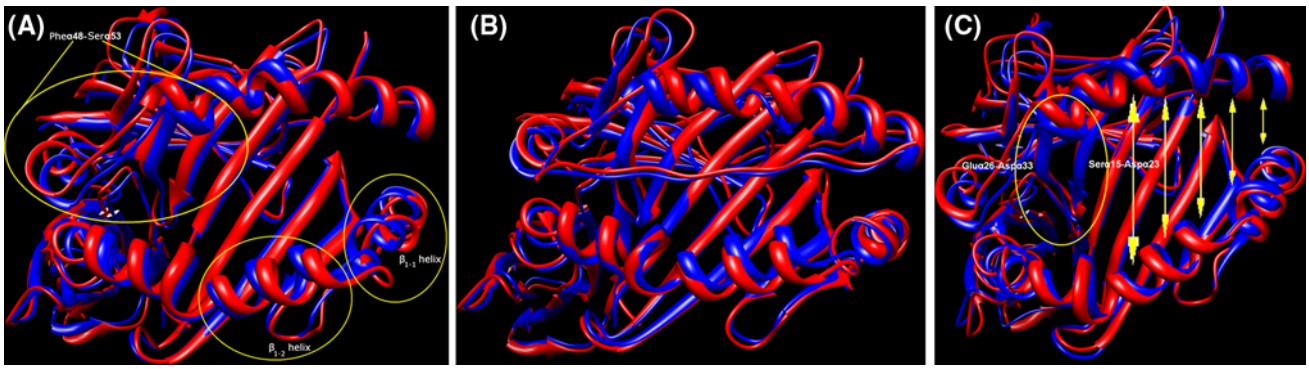

Fig. 7 Superimposition of initial structures of HLA-DRs Glyβ86 allelic variant (in *red*) with average simulated conformations obtained after 5 ns (in *blue*). **a** 1aqd_apo, **b** 1aqd_whole and **c** 1aqd_adcapy, AdCaPy is not shown in 1aqd_adcapy system. Transient conformational changes or opening near the N-terminus peptide-binding region, P1 pocket, has an overall influence towards stabilization of selected HLA-DR allelic variants. MHC class II empty-determinant antibody specific regions, β helices, have distorted geometry in peptide- and adcapy-loaded states

P4 pocket) and β_{1-2} (β65–74 relates with P6 pocket) helices near the C-terminus peptide groove have shown the same effect as observed in [54]. In contrast, the apo forms exhibit higher fluctuations, 1.12 and 1.14 Å for the 1aqd_apo and 1bx2_apo systems, respectively. The same β helices regions transit between folding and unfolding states toward the peptide-binding site causing the narrowness of the cleft. Antibody (KL295) specific for unbound Class II structures identifies the same high conformational helical mobility zone, in complete agreement with the experimental findings [10]. Region Pheα48-Serα53 is shifted towards the N-terminal region of the peptide-binding site to occupy the area of the peptide binding site. Such a small but significant change makes the 1aqd_apo form to be in the closed state. This is analogues to the motion of α50–59 region of HLA-DR1 (HLA-DRA*0101, HLA-DRB*0101) as revealed by molecular dynamics simulation studies [9]. The same region does not deviate as much in the 1bx2_apo system, although a region from the lower flanking helix (Alaβ49–Aspβ66) narrows in the direction of upper α flanking helix. This narrowness might provide hindrance for the incoming peptide (Figs. 7a, 8a). The void created by AdCaPy in the 1aqd_adcapy system clearly indicates its role as an MLE. The distance between the flanking helices increases to a much larger extent widening the peptide-binding site. Furthermore, the twisting of the floor of the β-strands (Serα15–Aspα23 and Gluα26–Aspα33) towards the interior offers greater opening of the peptide-binding cleft. A 1.09 Å deviation is observed for this system (Fig. 7c). It is remarkable to see that how a small compound creates such a space by widening the gap between parallel α-helices. The MLE effect of AdCaPy in the 1bx2_adcapy system is not observed, although it does distort the overall peptide-binding site. The relative $RMSD_{avg}$ value between the 1aqd_whole and 1aqd_adcapy systems is only 0.89 Å clearly demonstrating the overall structural similarity although there are two different binding modes. The C-terminal region of the antigenic binding site that forms the lower flanking helix region comes close to the upper α flanking helix. The whole system deviates 1.21 Å form the initial structure. Furthermore, the overall structure looks drastically changed except its binding site region (Fig. 8c).

Analysis of root mean square fluctuation (RMSF) of all simulated systems

Both the apo and whole 1AQD systems exhibit significant differences in their RMSF trends. The apo system has shown more conformational changes as compared to the peptide-loaded system. In the α subunit of 1AQD, the peptide-binding region (α47–73), which makes the helix part of the cleft, remains in constant high fluctuation. The same region in the peptide-loaded state fluctuated less. In the peptide-loaded state the β131–195 region has the least RMSF values as this region has satisfied all of its hydrogen bonding interactions with the bound peptide. In the 1aqd_adcapy system, the same region fluctuated as in the 1aqd_apo system but in the opposite direction. It moves further away form the α-helix. As a result, the distance between the two flanking α-helices increases due to the strain of interactions as caused by AdCaPy. This indicates that involvement of interacting amino acid residues eventually provides a way for the existence of AdCaPy as MLE in the allelic Glyβ86 cavity that further widens the peptide-binding cavity (Fig. 9; upper panel). In the same manner, if we compare the 1bx2_systems to each other, 1bx2_cmp exhibits constant fluctuations due to the complete conversion to the inactive state. Although, this transition has low RMSF values, continuous motion caused the structural disruption of the peptide-binding site into a more collapsed state (Fig. 9; lower panel).

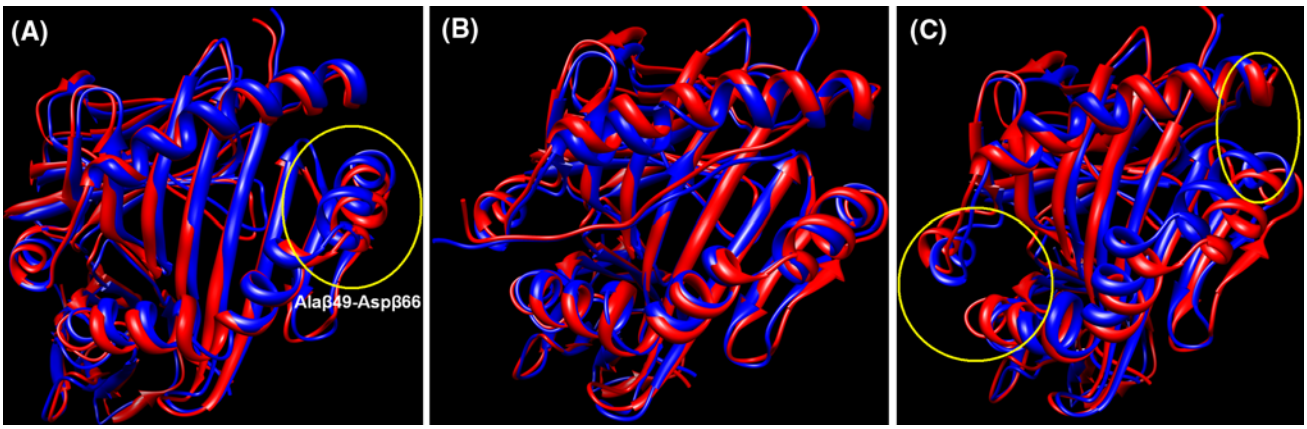

Fig. 8 Superimposition of initial structures of HLA-DRs Valβ86 allelic variant (in *red*) with average simulated conformations obtained after 5 ns (in *blue*). **a** 1bx2_apo, **b** 1bx2_whole and **c** 1bx2_adcapy, AdCaPy is not shown in 1bx2_adcapy system. Two *yellow circles* at each terminus of peptide-binding site (**c**) indicate closure or narrowing by decreasing distance between the flanking helices

Analysis of hydrogen bonding interactions

Trajectory analysis of all the hydrogen bonding interactions is depicted in Fig. 10. Snapshots of the conformations obtained after an interval of 1,000 ps are shown in Figs. 11 and 12. Figure 10 (upper panel) evidently shows that the hydrogen bonded interaction distances did not exhibit significant changes until 1,100 ps which suggests that the AdCaPy is residing efficiently in the predicted cavity. Interestingly, after 1,100 ps until the end of simulation time, all of the hydrogen bonds are broken and did not recover. The change in the binding pose of AdCaPy when the hydrogen bonds are broken (Fig. 11) reveals that the adamantine core group drills itself into the large Glyβ86 pocket. As it penetrates, its interactions with the hydrogen bonding amino acid residues are completely lost. This is the transition stage where side chain of AdCaPy lies outside the cavity whereas the adamantane core group resides within the cavity causes strain to the N-terminal region of the peptide-binding site which widens. This phenomenon not only prevents the Pheα48-Serα53 region to come close to the empty peptide-binding site but also the twisting of the β-strands (Serα15–Aspα23 and Gluα26–Aspα33) occurred. On the other hand, the hydrogen bonding interactions made by AdCaPy to the Valβ86 allelic variant are strong as compared to the 1aqd_adcapy system except for the hydrogen bond between the carbonyl O and the Ileα7:N4′. The involvement of Asnβ82 (Nδ2 Asnβ82:N1′ and Nδ2 Asnβ82:N2′) and Tyrβ78 (OH Tyrβ78:O1′) as hydrogen bonding partners (Fig. 10; lower panel) hold AdCaPy at that site. At the end of the simulation, these three hydrogen bonds persist which illustrates the presence of a suitable environment for AdCaPy. Such interactions cause structural instability in the peptide-binding site as the flanking helices are eventually disturbed (Fig. 12).

MD simulations support the hypothesis that the occupation of the P1 pocket prevents the closure of the empty peptide binding site which would produce the non-receptive peptide state. In other words, MLEs that bind in the dimorphic P1 pocket stabilize the receptive peptide state which enhances the display of antigenic peptides. It is clear from the RMSD fluctuation plots that the apo forms of both allelic pairs exhibit large structural changes as compared to any of the other studied systems. Since the dimorphic P1 pocket is vacant, the apo-protein is able to sample many conformational states, including collapsing the peptide binding site. Class II MHC molecules inactivate rapidly after the dissociation of the ligand, presumably converting them into a peptide non-receptive confirmation—reconversion back into a peptide receptive state is very slow. Adamantyl compounds are able to induce peptide receptive state.

In case of the 1aqd_apo system, major structural changes occurred in this allelic variant which favors the peptide non-receptive state. Since 1AQD has Gly at position β86, more structural rearrangements are needed to bring the protein to its inactive state. The flanking α helices are shifted away resulting in the narrowing of the peptide binding groove. This shifting is more prominent in P1 pocket, thus collapsing the region around this pocket. Comparatively, 1bx2_apo exhibits fewer structural variations since it has an already filled Valβ86 P1 pocket.

The 1aqd_adcapy system exhibits RMSD fluctuations very similar to the 1aqd_whole system indicating that AdCaPy prevents collapse of the P1 pocket, a desirable property of an MLE. The presence of AdCaPy in the predicted cavity stabilizes the protein conformation in such a way that the flanking α helices are now wide open to receive any incoming peptide, especially in the α1 domain region (α56–α70). The anti-parallel eight stranded β

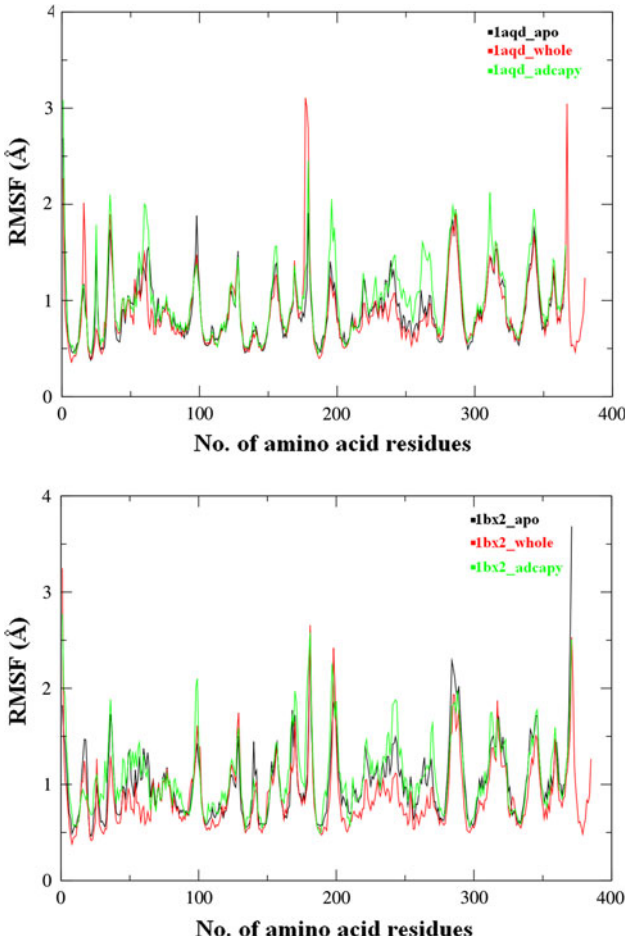

Fig. 9 RMSF values of polypeptide backbone (Cα, C, and N atoms) as a function of time in the production run for: 1aqd system; 1bx2 (*lower panel*). Numbering of amino acid residues starts from 1 (AMBER numbering) rather than from 2 for α chain and 3 for *β* chain

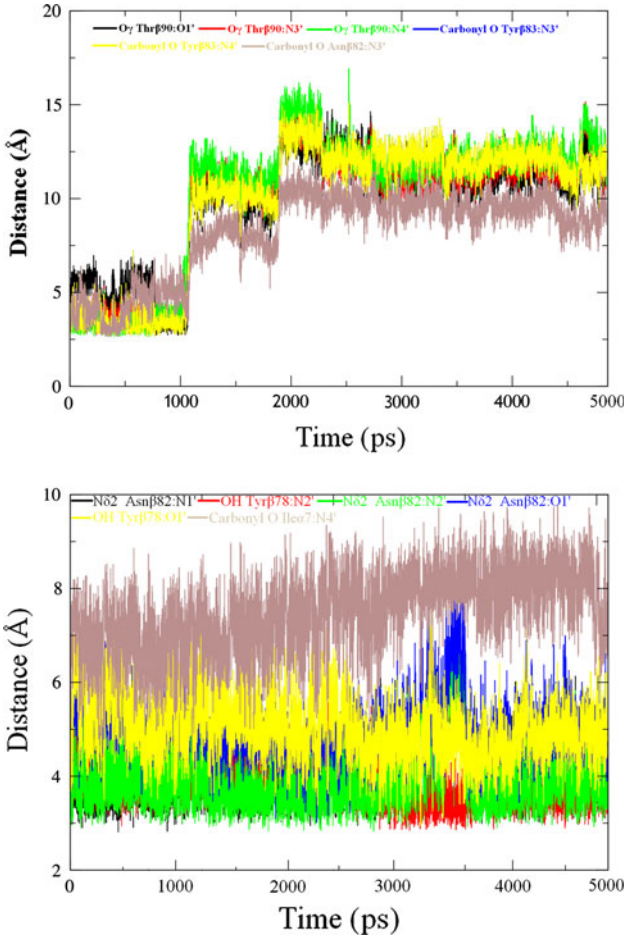

Fig. 10 Simulated trajectory analysis of hydrogen bonding interaction distances between atoms of HLA-DR Gly*β*86 (*upper panel*) and HLA-DR Val*β*86 (*lower panel*) with AdCaPy

pleated sheets are so well arranged that it forms a floor to accommodate peptides. The two ends of the peptide binding grooves are also significantly opened allowing the peptide to bind in an extended conformation. This permits peptides larger than the normal lengths to bind, such as tumor antigenic peptides. 1bx2_acapy is the system with the greatest fluctuations having an RMSD value around 3 Å. This is occurred because of the presence of Val*β*86 which only could not accommodate AdCaPy but also resulted in a shortening of the peptide binding groove from the peptide's amino and carboxyl ends. The α2 domain is largely affected due to the presence of the AdCaPy side chain which forms interactions with neighboring amino acid residues.

Conclusion

Previous studies have introduced MLEs as a new class of vaccine additives that increase $CD4^+$ cell responses by arbitrating effectual antigen loading of APC. Surface MHC II molecules of APCs are either blocked by high affinity peptide-ligands or have acquired a non-receptive peptide state. MLEs such as adamantyl derivatives are able to induce non-receptive MHC II molecules to 'open up' free binding sites by freeing ligands with lower affinity in an allele-dependent manner [19]. This characteristic feature of adamantyl derivatives allows a notable increase in the number of MHC II-antigen complexes on the cell surface of APCs. However, the cavity where these compounds bind and the molecular interactions they form with HLAD-Rs are not yet understood. This is the first study describing a putative cavity region in MHC II for any MLE. Furthermore, an in-depth molecular analysis of all six reported adamantyl derivates is presented. Special emphasis is given to AdCaPy in order to uncover structural changes during transition from peptide non-receptive to receptive conformations.

By now, several classes of compounds have been recognized as exhibiting MLE activity. In addition to organic molecules such as adamantyl derivatives or complex

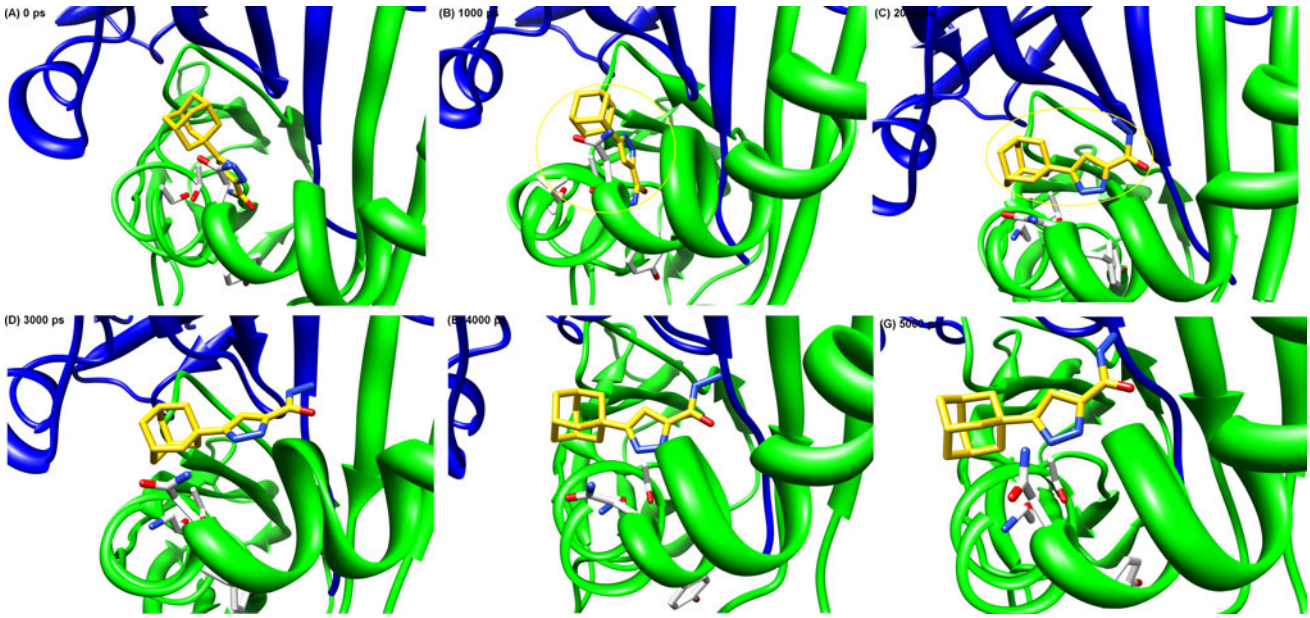

Fig. 11 Snapshots taken after an interval of 1,000 ps to observe transitional changes in 1aqd_adcapy system. Note the alteration in binding orientations of AdCaPy that occurred between 1,000 and 2,000 ps. At the end of simulation run time (G), AdCaPy side chain lies outside the cavity. *Blue ribbon* (α domain) and *green ribbon* (β domain)

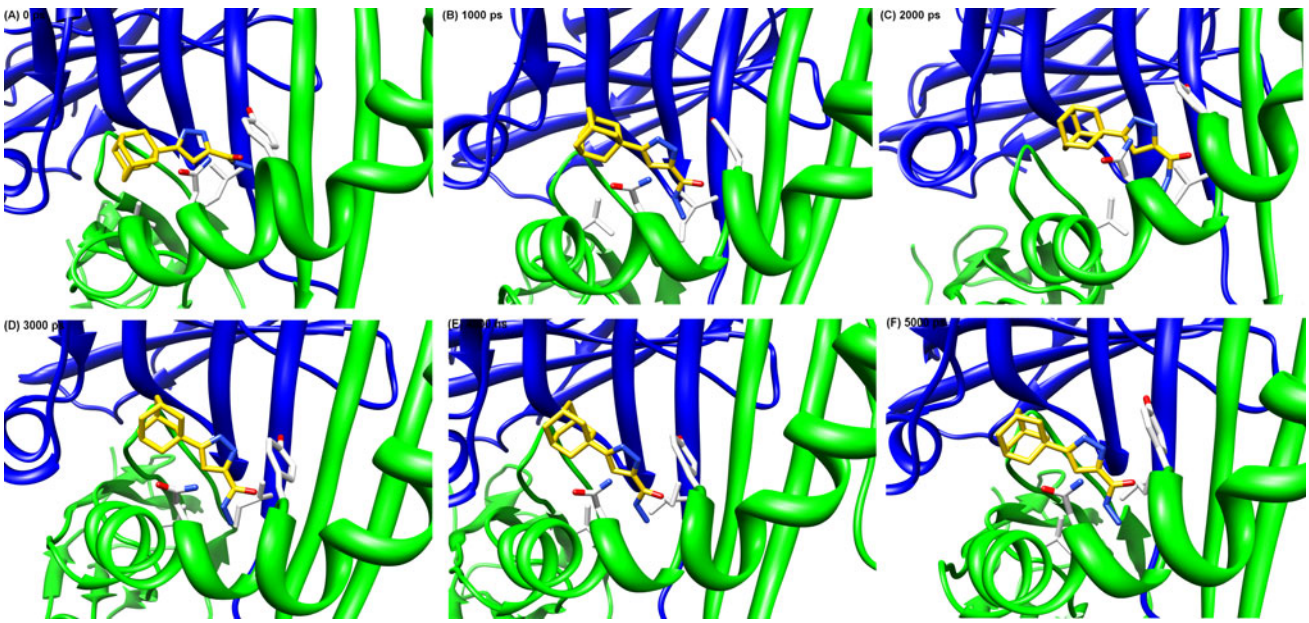

Fig. 12 Snapshots taken after an interval of 1,000 ps to observe transitional changes in 1bx2_adcapy system. Binding orientations of AdCaPy remain nearly constant. *Blue ribbon* (α domain) and *green ribbon* (β domain)

polycyclic compounds [18, 55], simple aromatic chemicals like p-chlorophenol [16, 17], short peptide derivatives [20] and even certain solvents such as ethanol and n-propanol [21] show this effect. But the disadvantage they had that all such chemicals act in a catalytic way independent of the antigen. More often, they can simply be added to the desired adjuvant and can be useful in most of the common protocols used for vaccination. Adamantyl derivatives are allele-dependent MLEs that can serve as vaccine candidates for TAA. So far, most of the reported tumor vaccines were aiming mainly at MHC class I. A number of recent studies confirmed, however, that immunizations concerning $CD4^+$ cells are more effective than peptide vaccinations targeting only $CD8^+$ cells [15, 56].

Cavity detection, molecular docking and molecular dynamics simulations of adamantly derivatives were

conducted to explore the features that may be responsible for mediating efficient peptide loading onto HLA-DRs allelic variants. All apo systems showed greater mobility particularly in the α- and β-helices that flank the binding groove region but no complete loss of α-helical secondary structure was noticed, indicating the local conformational change rather than the inconvergence of the system. AdCaPy is the first MLE compound whose dynamic behavior was examined resulted in a substantial stabilization of the complete peptide-binding pocket. This confirms that the presence of small organic compound that fills merely the N-terminus P1 binding pocket of class II MHC molecule can have a significant effect on the conformational sampling of the whole peptide-binding region. Asnβ82, Tyrβ83 and Thrβ90 are the only amino acid residues that play their part in activating the peptide-receptive state for HLA-DR Glyβ86 but Asnβ82 and Tyrβ78 provide much more consistent hydrogen bonding interactions to AdCaPy in case of HLA-DR Valβ86. Site-directed mutagenesis studies are further needed to identify, improve and rationalize the interactions of these compounds within the cavity.

Acknowledgments Authors gratefully acknowledge the valuable technical support provided by Prof. Bernd M. Rode (University of Innsbruck) during this research work. The authors are also grateful to the AMBER supporting team for providing AMBER software. Special thanks to Prof. James Briggs (University of Houston) for his valuable suggestions and proofreading the manuscript.

References

1. Corthay A, Skovseth DK, Lundin KU, Røsjø E, Omholt H, Hofgaard PO, Haraldsen G, Bogen B (2005) Immunity 22:371–383
2. Stern LJ, Potolicchio I, Santambrogio L (2006) Curr Opin Immunol 18:64–69
3. Watts C (2001) Curr Opin Immunol 13:26–31
4. McFarland BJ, Beeson C (2002) Med Res Rev 22:168–203
5. Stern LJ, Brown JH, Jardetzky TS, Gorga JC, Urban RG, Strominger JL, Wiley DC (1994) Nature 368:215–221
6. Brown JH, Jardetzky TS, Gorga JC, Stern LJ, Urban RG, Strominger JL, Wiley DC (1993) Nature 364:33–39
7. Hansen TH, Lybarger L, Yu L, Mitaksov V, Fremont DH (2005) Immunol Rev 207:100–111
8. Carven GJ, Chitta S, Hilgert I, Rushe MM, Baggio RF, Palmer M, Arenas JE, Strominger JL, Horejsi V, Santambrogio L (2004) J Biol Chem 279:16561–16570
9. Painter CA, Cruz A, López GE, Stern LJ, Zavala-Ruiz Z (2008) PLoS ONE 3:e2403
10. Zarutskie JA, Sato AK, Rushe MM, Chan IC, Lomakin A, Benedek GB, Stern LJ (1999) Biochemistry 38:5878–5887
11. Chou CL, Sadegh-Nasseri S (2000) J Exp Med 192:1697–1706
12. Rabinowitz JD, Vrljic M, Kasson PM, Liang MN, Busch R, Boniface JJ, Davis MM, McConnell HM (1998) Immunity 9:699–710
13. Schmitt L, Boniface JJ, Davis MM, McConnell HM (1999) J Mol Biol 286:207–218
14. Kalams SA, Walker BD (1998) J Exp Med 188:2199–2204
15. Hung K, Hayashi R, Lafond-Walker A, Lowenstein C, Pardoll D, Levitsky H (1998) J Exp Med 188:2357–2368
16. Marin-Esteban V, Falk K, Rötzschke O (2003) J Autoimmune 20:63–69
17. Marin-Esteban V, Falk K, Rotzschke O (2004) J Biol Chem 279:50684–50690
18. Nicholson MJ, Moradi B, Seth NP, Xing X, Cuny GD, Stein RL, Wucherpfennig KW (2006) J Immunol 176:4208–4220
19. Hopner S, Dickhaut K, Hofstatter M, Kramer H, Ruckerl D, Soderhall JA, Gupta S, Marin-Esteban V, Kuhne R, Freund C (2006) J Biol Chem 281:38535–38542
20. Gupta S, Höpner S, Rupp B, Günther S, Dickhaut K, Agarwal N, Cardoso MC, Kühne R, Wiesmüller KH, Jung G (2008) PLoS ONE 3:e1814
21. Falk K, Lau JM, Santambrogio L, Esteban VM, Puentes F, Rötzschke O, Strominger JL (2002) J Biol Chem 277:2709–2715
22. Jones EY, Fugger L, Strominger JL, Siebold C (2006) Nat Rev Immunol 6:271–282
23. Pinet V, Vergelli M, Martini R, Bakke O, Long EO (1995) Nat 375:603–606
24. Vergelli M, Pinet V, Vogt AB, Kalbus M, Malnati M, Riccio P, Long EO, Martin R (1997) Eur J Immunol 27:941–951
25. Santambrogio L, Sato AK, Carven GJ, Belyanskaya SL, Strominger JL, Stern LJ (1999) Proc Natl Acad Sci 96:15056–15061
26. Santambrogio L, Sato AK, Fischer FR, Dorf ME, Stern LJ (1999) Proc Natl Acad Sci 96:15050–15055
27. Dickhaut K, Hoepner S, Eckhard J, Wiesmueller KH, Schindler L, Jung G, Falk K, Roetzschke O (2009) PLoS One 4:e6811
28. Warren GL, Andrews CW, Capelli AM, Clarke B, LaLonde J, Lambert MH, Lindvall M, Nevins N, Semus SF, Senger S (2006) J Med Chem 49:5912–5931
29. International hwtcT
30. Gasteiger J, Marsili M (1980) Tetrahedron 36:3219–3228
31. Clark M, Cramer RD, Opdenbosch NV (1989) J Comp Chem 10:982–1012
32. Berman HM (2007) Acta Cryst 64:88–95
33. Murthy VL, Stern LJ (1997) Struct 5:1385–1396
34. Stern LJ, Wiley DC (1994) Structure 2:245–251
35. Smith KJ, Pyrdol J, Gauthier L, Wiley DC, Wucherpfennig KW (1998) J Exp Med 188:1511–1520
36. Li Y, Li H, Martin R, Mariuzza RA (2000) J Mol Biol 304:177–188
37. Thomsen R, Christensen MH (2006) J Med Chem 49:3315–3321
38. Z M (1992) Spinger, Berlin
39. Michalewiez ZFD (2000) How to solve it: modern heuristics. Spinger, Berlin
40. Gehlhaar DK, Verkhivker G, Rejto PA, Fogel DB, Fogel LJ, Freer ST (1995) In: McDonnell JR, Reynolds RG, Fogel DB (eds) Proceedings of the fourth international conference on evolutionary programming. Massachusetts Institute of Technology, USA
41. Gehlhaar DK, Bouzida D, Rejto PA (1998) In: Porto VW, Saravanan N, Waagen DE, Eiben AE (eds) Proceedings of the seventh international conference on evolutionary programming. Springer, USA
42. Yang JM, Chen CC (2004) Proteins 55:288–304
43. Aaqvist J (1990) J Phys Chem 94:8021–8024
44. Case DA, Cheatham TE III, Darden T, Gohlke H, Luo R, Merz KM Jr, Onufriev A, Simmerling C, Wang B, Woods RJ (2005) J Comp Chem 26:1668–1688
45. Wang J, Wolf RM, Caldwell JW, Kollman PA, Case DA (2004) J Comp Chem 25:1157–1174
46. Essmann U, Perera L, Berkowitz ML, Darden T, Lee H, Pedersen LG (1995) J Comp Phys 103:8577–8593
47. Ryckaert JP, Ciccotti G, Berendsen HJC (1977) J Comp Phys 23:327–341

48. Humphrey W, Dalke A, Schulten K (1996) J Mol Graph 14:33–38
49. Pettersen EF, Goddard TD, Huang CC, Couch GS, Greenblatt DM, Meng EC, Ferrin TE (2004) J Comp Chem 25:1605–1612
50. O'Sullivan D, Arrhenius T, Sidney J, Del Guercio MF, Albertson M, Wall M, Oseroff C, Southwood S, Colon SM, Gaeta FC (1991) J Immunol 147:2663–2669
51. Geluk A, Van Meijgaarden KE, Southwood S, Oseroff C, Drijfhout JW, De Vries RR, Ottenhoff TH, Sette A (1994) J Immunol 152:5742–5748
52. Falk K, Rötzschke O, Stevanovíc S, Jung G, Rammensee HG (1994) Immunogenetics 39:230–242
53. Vaught A (1996) Linux J 1996:7
54. Yaneva R, Springer S, Zacharias M (2009) Biopolymers 91:14–27
55. Call MJ, Xing X, Cuny GD, Seth NP, Altmann DM, Fugger L, Krogsgaard M, Stein RL, Wucherpfennig KW (2009) J Immunol 182:6342–6352
56. Toes REM, Ossendorp F, Offringa R, Melief CJM (1999) J Exp Med 189:753–756